NACA TN 4236 10577

TECH LIBRARY KAFB, NM
0066806

NATIONAL ADVISORY COMMITTEE FOR AERONAUTICS

TECHNICAL NOTE 4236

EFFECTS OF MACH NUMBER AND WALL-TEMPERATURE RATIO ON TURBULENT HEAT TRANSFER AT MACH NUMBERS FROM 3 TO 5

By Thorval Tendeland

Ames Aeronautical Laboratory
Moffett Field, Calif.

Washington
April 1958

TECHNICAL NOTE

TECH LIBRARY KAFB, NM
0066806

NATIONAL ADVISORY COMMITTEE FOR AERONAUTICS

TECHNICAL NOTE 4236

EFFECTS OF MACH NUMBER AND WALL-TEMPERATURE RATIO ON TURBULENT HEAT TRANSFER AT MACH NUMBERS FROM 3 TO 5

By Thorval Tendeland

SUMMARY

Heat-transfer data were evaluated from temperature time histories measured on a cooled cylindrical model with a cone-shaped nose and with turbulent flow at Mach numbers 3.00, 3.44, 4.08, 4.56, and 5.04. The experimental data were compared with calculated values using a modified Reynolds analogy between skin friction and heat transfer. Theoretical skin-friction coefficients were calculated using the method of Van Driest and the method of Sommer and Short.

The heat-transfer data obtained from the model were found to correlate when the T' method of Sommer and Short was used. The increase in turbulent heat-transfer rate with a reduction in wall to free-stream temperature ratio was of the same order of magnitude as has been found for the turbulent skin-friction coefficient.

INTRODUCTION

With the emphasis on higher and higher speeds for modern aircraft, the effects of aerodynamic heating and the importance of being able to predict the rates of heat transfer are well recognized. For laminar flow the method of predicting heat transfer is fairly accurate and reliable; however, for turbulent flow there still exists an uncertainty with regard to evaluating heat transfer.

For subsonic turbulent flow the correlation between heat transfer and skin friction by means of Reynolds analogy has been well established. For supersonic flow a modified Reynolds analogy relating heat transfer and skin friction has been presented by Rubesin in reference 1. Considerable skin-friction data have been correlated in reference 2. The results of these two references can be used for predicting turbulent heat transfer. An alternative method is to use the theoretical work of Van Driest (ref. 3). These methods predict heat transfer for turbulent air flow with a zero pressure gradient.

A considerable amount of turbulent heat-transfer data has been reported, for example, references 4 through 11. However, the majority

of the investigations were conducted at relatively low Mach numbers and with low heat transfer or with wall temperatures near recovery temperatures. The data of reference 2 show a large increase in skin friction with an increase in heat transfer.

The purpose of this investigation was to obtain turbulent heat-transfer data at various Mach numbers and at various ratios of wall to free-stream temperature and to check the prediction, based on skin-friction measurements of reference 2, that a decreasing wall-temperature ratio causes a large increase in heat transfer or Stanton number.

SYMBOLS

A	surface area
C_F	average skin-friction coefficient, $\frac{1}{x}\int_0^x c_f \, dx$
c_f	local skin-friction coefficient, $\frac{\text{local shear}}{\frac{1}{2}\rho_1 u_1^2}$
c_p	specific heat of air at constant pressure
h	local heat-transfer coefficient, $\frac{q}{T_r - T_w}$
M	Mach number
p	pressure
q	local heat-transfer rate per unit area
R	Reynolds number, $\frac{u_1 \rho_1 x}{\mu_1}$
r	recovery factor, $\frac{T_r - T_1}{T_0 - T_1}$
S	Sutherland constant (see eq. (9))
St	Stanton number, $\frac{h}{\rho_1 u_1 c_p}$
T	absolute temperature
t	time
u	air velocity
x	effective distance along the model
ϵ	emissivity

τ_m thickness of model material

σ Stefan-Boltzmann constant, 0.173×10^{-8} Btu/(hr)(sq ft)($^\circ$R)^4

ρ density of air

ρ_m density of model material

μ coefficient of viscosity

Subscripts

av average

i incompressible

n condition at nitrogen spray tube

o stagnation value

r conditions at surface for zero heat transfer

t conditions at tunnel wall

w conditions at surface of model

1 local stream condition at outer edge of boundary layer

∞ undisturbed free-stream conditions

Superscripts

' conditions at which incompressible flow relations must be evaluated in order to represent compressible flow

w exponent for the temperature-ratio variation of viscosity

DESCRIPTION OF EQUIPMENT

Wind Tunnel

The investigation was conducted in the Ames 10-inch heat-transfer wind tunnel which is a variable-pressure, variable-temperature, continuous-flow type with a Mach number range from 3 to 5. A schematic diagram is shown in figure 1.

Model

Two models were used in the investigation: a pressure-distribution model to measure surface pressures and a temperature-distribution model. A sketch of the two models is shown in figure 2. Both models consisted of a 2-inch-diameter cylindrical body approximately 14-3/4 inches long and equipped with a 20° included-angle nose section. At nine longitudinal stations on the cylindrical portion of the pressure-distribution model there were pressure taps. Two pressure taps were located on the nose section of the model, one on the top surface and one diametrically opposite on the bottom surface. Surface pressures were measured on a dibutylphthalate manometer.

The temperature-distribution model was fabricated from type 321 stainless steel. Considerable care was taken in the machining of this model in order to obtain a uniform diameter and a uniform wall thickness. The cylindrical section had a wall thickness of 0.065 inch. The wall of the cone-shaped nose varied in thickness from 0.125 inch at the base to 0.166 inch at 1 inch from the tip. There was a 1/4-inch-diameter stainless-steel tube along the model axis. The purpose of this tube was to cool the model by spraying the inner walls with liquid nitrogen. This tube was equipped with approximately 140 small orifices varying in diameter from 0.016 to 0.040 inch. The spacing and size of the holes were selected on the basis of preliminary tests to obtain a constant temperature along the model.

The model was instrumented with 20 constantan-nichrome thermocouples. Eighteen of the thermocouples were located on the cylindrical portion of the model, with three thermocouples at each of six stations. The other two thermocouples were spaced along the nose cone of the model. The thermocouples were imbedded in the inner wall by means of a high-temperature solder and the leads were brought out at the rear of the model. The thermocouple leads within the model were supported and separated from the nitrogen spray tube by means of thin cross-shaped supports made from a Fiberglas material. The size of the thermocouple wire was No. 30 B and S gage for the constantan wire and No. 32 B and S gage for the nichrome wire. These thermocouple materials were chosen because of their reasonably good millivolt temperature relationship and their relative insensitivity to changes in resistance with changes in temperature. Time histories of the wall temperature were obtained by recording the thermocouple outputs on an oscillograph. Very little data was obtained at station 1 on the model as a result of the thermocouples breaking at this station when the tunnel air flow was started and stopped. The conditions for the various tests are as follows:

M_∞	T_o, °F	p_o, psia	R_1/ft, million
3.00	395	37.5	3.0
3.44	407	55.0	4.0
4.08	410	81.6	3.6
4.56	415	83.0	2.8
5.04	415	85.7	2.3

Boundary-Layer Trip

For all of the tests a boundary-layer trip made from 1-50-D garnet paper, with most of the backing removed, was used. A strip of this paper approximately 1/2 inch wide was fastened to the nose of the model, 1/2 inch from the tip. With this trip, turbulent recovery temperature was measured at all thermocouple stations at Mach numbers up to 5. For the tests at a Mach number 5 it was necessary to resort to two of these trips, the second one located approximately 1/4 inch downstream from the first trip.

Liquid Nitrogen Equipment

The equipment used to bring the liquid nitrogen into the model is shown schematically in figure 3. It consisted of an insulated stainless-steel tank which was filled from flasks used to store and transport the liquid nitrogen. The liquid nitrogen was forced into the model by pressurizing the stainless-steel tank with gaseous nitrogen. A three-way valve was used in the line between the model and the stainless-steel tank. It was necessary to shut off the liquid nitrogen supply before taking temperature data; the three-way valve permitted this to be done quickly. Also by connecting the third passage from the valve to a low-pressure region in the test section the residual liquid nitrogen in the supply line to the model could be purged rapidly. At the higher Mach numbers the model could not be cooled to as low a temperature as desired because of the method of removing the coolant from the model. This method was to exhaust the coolant into the wind-tunnel air stream at the rear of the model. The amount of coolant which the wind-tunnel air stream could absorb without choking decreased as the Mach number was increased. Therefore since the model wall temperature was dependent on the amount of coolant that was used, the necessity of reducing the quantity of coolant to prevent choking of the wind tunnel resulted in less cooling (higher model wall temperatures) at the higher Mach numbers.

REDUCTION OF DATA

Determining Heat-Transfer Rates

Heat-transfer rates were evaluated from temperature time histories of the model by means of the following heat balances:

$$q_{model} = (q_{convection}) + (q_{radiation\ from\ tunnel\ wall}) - (q_{radiation\ to\ nitrogen\ spray\ tube})$$

or more explicitly from reference 12,

$$\rho_m \tau_m A_w \frac{dT_w}{dt} = hA_w(T_r - T_w) + \frac{A_w\sigma\left[\left(\frac{T_t}{100}\right)^4 - \left(\frac{T_w}{100}\right)^4\right]}{\frac{1}{\epsilon_w} + \frac{A_w}{A_t}\left(\frac{1}{\epsilon_t} - 1\right)} - \frac{A_n\sigma\left[\left(\frac{T_w}{100}\right)^4 - \left(\frac{T_n}{100}\right)^4\right]}{\frac{1}{\epsilon_n} + \frac{A_n}{A_w}\left(\frac{1}{\epsilon_w} - 1\right)} \tag{1}$$

No corrections were made in the above equation for axial or circumferential conduction along the model. An estimate of the effects of conduction was made using the temperature gradients as measured and it was found that this correction amounted to approximately 3 percent of the convective heat-transfer rate at the worst condition, Mach number 5. For lower Mach numbers the correction was less. Therefore, the effects of axial conduction were neglected.

To evaluate the heat transferred by radiation to the model an emmissivity of 0.2 was used for the polished outer surface of the model. This value was obtained from reference 13. For the inner surface of the model, the nitrogen spray tube, and the tunnel walls, an emissivity value of 0.5 was used since these surfaces were discolored and tarnished from heating. The specific heat of the model and its variation with temperature were obtained from data given in reference 14 for type 347 stainless steel. The model was fabricated from type 321 stainless steel; however, these two types of stainless steel are practically identical in composition, the main difference being that one is stabilized with a small amount of titanium and the other with columbium. The theoretical specific heats of the two types of stainless steel were compared by means of Kopp's rule (ref. 15) and no significant difference could be determined.

In equation (1) the major problem is evaluating the rate of change of model wall temperature with time. To evaluate this rate of change two methods were used. The method which was used most extensively was to determine an average slope for a small time interval by means of the ratio $\Delta T_w/\Delta t$. Temperatures at the end of each time interval were determined from deflections taken from the oscillograph records. An average wall temperature for the time interval was used to determine the radiation correction and the ΔT between the model and the recovery temperature.

A second method was to plot the wall temperature versus time, fair a curve through the data, and determine slopes by means of a mirror. Both methods gave essentially the same results. A comparison of heat-transfer data as evaluated by both methods is given in the discussion of results. No reduction of temperature data to determine heat-transfer coefficients for the nose section was undertaken because of uncertainties associated with the wall thickness and also because of the effects of axial heat conduction with the relatively thick wall.

Evaluating a Local Reynolds Number

On a flat plate with a boundary-layer trip located near the leading edge, one would expect the effective origin for turbulent flow to be located some distance upstream from the trip location. This location would depend upon the length of run of laminar boundary layer preceding the boundary-layer trip plus the increase in momentum thickness of the boundary layer caused by the trip. On the present model, however, the nose section was a cone and the rate of growth of the boundary layer and conditions of flow are different from those on a flat plate. The boundary-layer growth on the cylindrical section should correspond approximately to that on a flat plate (ref. 16).

It was calculated that the nose cone moved the effective origin for turbulent flow downstream approximately 2-1/2 inches from where it would have been if the model were cylindrical throughout its length. In the calculations, local skin-friction coefficients over the nose section were determined on the assumption that turbulent flow originated at the tip of the model. A length which would give equivalent turbulent skin-friction coefficients for a flat plate was then evaluated. In the calculations, Mach numbers and conditions of flow corresponded to those on the model. To obtain additional information regarding the location of the effective origin of the turbulent boundary layer, local Stanton numbers for the various stations along the model were plotted versus Reynolds numbers based on several assumed locations of the origin of the turbulent boundary layer. The slopes of curves faired through the data were then compared to the slopes as determined by the method given in Appendix A. The best agreement between the slopes was found when the effective origin for turbulent flow was located at the nose of the model. No significant difference could be detected for the various Mach numbers. Therefore, for all of the tests local Reynolds numbers were calculated with the effective origin for turbulent flow located at the tip of the model. The exact location of the effective origin for turbulent flow does not have a large effect on the calculated local Stanton number for these tests, because the model was fairly long and because Stanton number does not vary greatly with Reynolds number. For example, a difference of 2-1/2 inches in the location of the origin of the turbulent boundary layer would cause a change in Stanton number of approximately 3 to 6 percent, depending upon the location on the model.

Determining Local Flow Conditions

Local values for Mach number, temperature, and density along the body were computed from the measured pressure distributions on the assumption that the total pressure was constant along the body and equal to the calculated pressure behind the shock wave at the nose of the model. No extraneous shock waves which might affect the flow or the assumption of constant total pressure along the model could be detected from pressure measurements or from schlieren pictures. Free-stream Mach number upstream of the shock wave at the nose of the model was evaluated from the ratio of stagnation pressure to tunnel side-wall static pressure and also from the ratio of the surface pressure on the nose cone to stagnation pressure.

RESULTS AND DISCUSSION

Air Flow and Temperature-Distribution Results

Pressure and Mach number distributions.- In figure 4 are shown the pressure distributions which were measured on the pressure-distribution model for free-stream Mach numbers 3.00, 3.44, 4.08, 4.56, and 5.04. These are the Mach numbers at which the heat-transfer tests were run. (Pressure distributions also were measured when the model was equipped with a boundary-layer trip consisting of two 0.010-inch-diameter wires spaced along the nose. No effect of the trip could be detected on the surface pressures.) Shown in figure 4 are the theoretical pressure distributions of reference 17 for Mach numbers 3, 4, and 5. Predictions were not available for Mach numbers 3.44 and 4.56. The agreement of the data with the predictions of reference 17 is fair. In figure 5 are the Mach number distributions along the model which were calculated from the measured pressure distributions (fig. 4). The Mach number variation along the cylindrical portion of the model was approximately 6 percent of the free-stream Mach number. This is not a large change in Mach number. Shown in figure 5 also are values for the free-stream Mach number as determined from tunnel side-wall pressure taps and also from pressures measured on the nose cone of the model. Mach number as determined from these two methods was in good agreement; also, the Mach number variation along the test section was not large.

Temperature and recovery-factor distributions.- Typical axial-temperature distributions for the heat-transfer model during a temperature time-history run are shown in figure 6 for each of the test Mach numbers. The temperature distributions labeled "start of run" were measured after the model was cooled, the liquid nitrogen was shut off, and the model wall temperature was rising. Before cooling, the model was run in the wind tunnel for a considerable length of time in order to reach equilibrium temperature conditions and eliminate temperature gradients along the model. As may be noted from figure 6, for Mach numbers 3,00, 3.44, and 4.08 the temperature distributions at the start of the runs were similar

and had a random scatter of approximately 12 percent of the temperature potential for heat transfer. As the model temperature increased, it became more uniform and the rate of temperature rise of the model was approximately the same throughout its length. The heat-transfer rate on the nose cone was more than double the rate on the cylindrical section but the wall thickness of this section was increased to compensate for this higher rate of heat transfer.

Recovery factors as evaluated from temperatures measured along the model are shown also in figure 6. These temperatures were obtained prior to a cooling run when the model was at an equilibrium condition. After corrections were made for a small amount of radiant heat transfer to the cooler tunnel side walls, these local temperatures together with the local Mach number and the measured stagnation temperature permitted local recovery factors to be calculated. An examination of figure 6 for test Mach numbers 3.00, 3.44, and 4.08 shows values for recovery factors of approximately 0.88 to 0.89. These values when compared to values of 0.85 to 0.86 for laminar air flow clearly indicate turbulent air flow over the model. The recovery factors on the nose cone were slightly lower than those on the cylindrical section, a result which also was found in the tests of reference 18.

For Mach numbers 4.56 and 5.04 the temperature distributions and recovery factors along the model become somewhat different. The difference is that temperatures and recovery factors on the cylindrical section near the junction of the cone section were less than for the rest of the model. As may be noted from figure 6 for Mach numbers 4.56 and 5.04 the recovery factors on the nose section and toward the rear portion of the model are values for turbulent flow. However, near the junction of the nose section, the values for recovery factor are reduced and approach in magnitude values for laminar flow. Similar results have been published in reference 18. Model wall temperatures in the vicinity of the shoulder were also less than those on the rest of the model. The cause of this phenomenon may be associated with the large reductions in surface pressures which occur at the junction between the nose cone and the cylindrical afterbody and are shown in figure 4.

Since all of the theories used to predict heat transfer are based on an isothermal wall, there is the effect of axial-temperature gradients, such as shown in figure 6, on the heat-transfer results. The effects of axial-temperature gradients on local Stanton number were calculated by the method given in reference 19. For Mach numbers 3.00, 3.44, and 4.08 the axial-temperature gradients would have a small effect on the data. However, at Mach numbers 4.56 and 5.04 the abrupt reduction in wall temperature near the shoulder of the cone and the cylindrical section would cause turbulent heat-transfer data in this region to be in error approximately 10 to 15 percent. Since the flow in this region appears to be neither laminar nor turbulent, no attempt was made to correlate these data.

Heat-Transfer Results

Correlation of Stanton number with Reynolds number.- Experimentally determined values of Stanton number are plotted as a function of Reynolds number in figure 7 for constant wall-temperature ratios and for each of the five test Mach numbers. The variations in Reynolds number are due to the different values of length from the start of turbulent flow for each thermocouple station. For each Mach number the tests were run at the highest pressure level or Reynolds number which could be obtained from the wind-tunnel equipment; also, because of the difficulty in obtaining turbulent flow along the entire length of the model no attempts were made to obtain heat-transfer data at lower stagnation pressures or lower Reynolds numbers. For comparison theoretical curves of Stanton number are also shown in figure 7. To calculate the theoretical curves, the methods of Van Driest (ref. 3) and of Sommer and Short (ref. 2) were used to evaluate skin friction and the correlation between skin friction and heat transfer was based on the modified Reynolds analogy of Rubesin (ref. 1). The basis of the method of Sommer and Short is the Kármán-Schoenherr incompressible flow equation for average skin friction which is

$$\frac{0.242}{C_F} = \log_{10}(C_F R) \tag{2}$$

but where the density and viscosity of the air are evaluated at a temperature T' rather than T_1. The equation for T' which has been found to correlate the skin-friction data for turbulent flow (ref. 2) is

$$\frac{T'}{T_1} = 1 + 0.035M_1^2 + 0.45\left(\frac{T_w}{T_1} - 1\right) \tag{3}$$

An examination of figure 7 shows that the data for Mach numbers 3.00, 3.44, and 4.08, although having considerable scatter, have approximately the same slope as the theoretical curves; also, these data are in better agreement with the calculated curves when the method of Sommer and Short is used than when the method of Van Driest is used. For Mach number 4.56 at station 2 and for Mach number 5.04 at stations 2 and 3 the values of Stanton number are low compared to the theoretical curves. These low values of Stanton number are associated with the low rate of temperature rise and the low recovery factors as measured at these stations and as noted in figure 6. It is interesting to note that the fully turbulent heat-transfer data at Mach numbers 4.56 and 5.04 in figure 7 correlate with a Reynolds number based on a length beginning at the nose of the model. This would indicate that so far as heat transfer is concerned the effective origin of the turbulent boundary layer is unaffected by the flow conditions in the vicinity of the shoulder. For comparison with the data obtained with the model internally cooled, a limited amount of heat-transfer data was also obtained with the model externally cooled. For these tests liquid nitrogen was sprayed into the wind-tunnel air

stream at the center line of the subsonic portion of the nozzle. The cool nitrogen introduced into the hot tunnel air stream cooled the center core of the air stream which, in turn, cooled the model to approximately 175° F below recovery temperature. The nitrogen was then shut off and temperature time histories of the model wall were taken. Values of Stanton number determined from the temperature data for Mach numbers 4.08 and 4.56 are shown in figure 7. These data are in fair agreement with those obtained with the model internally cooled.

The effect of wall-temperature ratio on Stanton number.- Since one of the main objectives of this investigation was to obtain heat-transfer data with variable wall temperatures, a plot of local Stanton number versus wall to free-stream temperature ratio is shown in figure 8. The data shown in figure 8 were obtained at station 4 and are representative of all the data. For comparison with the data, curves calculated by the methods of references 2 and 3 are also shown in figure 8. The effect of a decrease in wall-temperature ratio was to increase the heat-transfer rate. The curves calculated by the methods of Sommer and Short and of Van Driest also show an increase in heat transfer with decreasing wall-temperature ratio, with the predictions by the Sommer and Short method showing the greatest effect of wall-temperature ratio. In figure 8 the data also appear to be in better agreement with the predictions made by the method of Sommer and Short.

Shown in figure 8 for a Mach number 3.00 are two sets of data both for the same thermocouple but, the slopes were determined for one set by means of a mirror and for the other set by the use of the ratio $\Delta T_w/\Delta t$. As may be noted from this figure determining slopes by either of the two methods results in essentially the same value of Stanton number.

Correlation of test data on the basis of St' and R'.- As a result of the agreement of the data in figures 7 and 8 with the curves calculated by means of the correlation of Sommer and Short, all of the fully turbulent data were correlated on the basis of St' versus R'. This correlation is shown in figure 9. The prime superscript indicates that the density and viscosity of the air were evaluated at a temperature T'. The relationship between St and St' is as follows:

$$St = \frac{h}{\rho_1 u_1 c_{p_1}} = \frac{h}{\rho' u_1 c_{p'}} \left(\frac{\rho' u_1 c_{p'}}{\rho_1 u_1 c_{p_1}} \right) \tag{4}$$

Since $c_{p'} \cong c_{p_1}$

$$St = St' \left(\frac{\rho'}{\rho_1} \right) = St' \left(\frac{T_1}{T'} \right) \tag{5}$$

or

$$St' = St \left(\frac{T'}{T_1} \right) \tag{6}$$

and as noted previously

$$\frac{T'}{T_1} = 1 + 0.035M_1^2 + 0.45\left(\frac{T_w}{T_1} - 1\right)$$

the relationship between R_1 and R' is

$$\frac{R'}{R_1} = \left(\frac{\rho'}{\rho_1}\right)\left(\frac{\mu_1}{\mu'}\right) \tag{7}$$

or

$$R' = R_1 \frac{1}{\left(\frac{T'}{T_1}\right)\left(\frac{\mu'}{\mu_1}\right)} \tag{8}$$

and where μ'/μ_1 can be determined from the Sutherland equation, or

$$\frac{\mu'}{\mu_1} = \left(\frac{T'}{T_1}\right)^{1.5}\left(\frac{T_1 + S}{T' + S}\right) \tag{9}$$

The curves shown in figure 9 were calculated by means of the analogy between skin friction and heat transfer of reference 1 with local skin friction evaluated by the incompressible flow equation of Von Kármán and Schoenherr which is

$$c_f = \frac{0.558\ C_F}{0.558 + 2\sqrt{C_F}} \tag{10}$$

and for average skin friction

$$\frac{0.242}{\sqrt{C_F}} = \log_{10} R_x C_F \tag{11}$$

If the correlation of St' and R' is used, the data for all Mach numbers and all wall-temperature ratios should correlate with one curve. In figure 9 separate plots of data were shown for each of the Mach numbers in order to simplify the presentation of the data and to note any trend or difference between the various Mach numbers. An examination of figure 9 shows that although the data have considerable scatter the agreement with the curve is quite good for all Mach numbers. A simplified equation for St' which correlates the data and fits the curve shown in figure 9 within 2 to 3 percent over the Reynolds number range from 100,000 to 10,000,000 is

$$St' = \frac{0.026}{(R')^{0.18}} \tag{12}$$

Correlation of test data on the basis of St/St_i with T'/T_1.- All of the turbulent heat-transfer data obtained are plotted in figure 10 as St/St_i versus T'/T_1. The values of St_i were calculated by means of the Kármán-Schoenherr equation for skin friction together with the modified Reynolds analogy of reference 1. The curve shown in figure 10 was calculated by the method given in reference 2 and the relationship

$$\frac{St}{St_i} = \frac{C_F}{C_{F_i}}$$

A simplified equation for the relationship of St/St_i to T'/T_1 is given in Appendix B. An examination of figure 10 shows that the heat-transfer data for all five Mach numbers and for all ratios of T'/T_1 agree well with the skin-friction correlation as represented by the curve. The method of least squares was used to fit a curve to the data and it was found that the maximum deviation between this curve and the theoretical curve shown in figure 10 was approximately 4 percent in the values of St/St_i.

As a result of the correlation of the data with the ratio T'/T_1, a similar analogy was applied to the results of other heat-transfer investigations and is shown in figure 11. The data shown in figure 11 for the different investigations are not complete sets but were chosen to be representative of the results of the particular investigation. The curve shown in figure 11 is the same curve as shown in figure 10. The data plotted in figure 11 show scatter which is typical of heat-transfer measurements but they also follow the general pattern of substantiating the skin-friction correlation of reference 2. At the higher Mach numbers (i.e., higher ratios of T'/T_1), the data of Lobb, Winkler, and Persh (ref. 6) are low as compared to the calculated curve. Other data available for the higher Mach numbers are not sufficiently complete to enable correlation in this manner.

CONCLUSIONS

Heat-transfer data were evaluated from temperature time histories measured on a cooled cone-cylinder model with a turbulent boundary-layer. The results can be summarized as follows:

1. The ratio of wall to free-stream temperature has an appreciable effect on the heat-transfer rate and the increase in heat-transfer rate with decreasing wall-temperature ratio is equivalent to the increase in turbulent skin-friction coefficient which has been measured previously.

2. The T' method used by Sommer and Short to correlate turbulent skin-friction data with Mach number and wall-temperature ratio has been found to correlate the turbulent heat-transfer data of this investigation.

Ames Aeronautical Laboratory
National Advisory Committee for Aeronautics
Moffett Field, Calif., Jan. 28, 1958

APPENDIX A

DETERMINING SLOPE OF STANTON NUMBER VERSUS REYNOLDS NUMBER CURVE

The results of reference 2 for a given Mach number and wall-temperature ratio have shown that C_F/C_{F_i} is a constant, with the exception of a small dependence on Reynolds number. On the basis of the analogy between skin friction and heat transfer the same conclusion is indicated with regard to the ratio, St/St_i. If the effect of Reynolds number, which is small for the range of the test conditions, is neglected, then

$$\frac{St}{St_i} = \text{constant} \tag{A1}$$

When equation (12) is applied to incompressible flow it reduces to

$$St_i = \frac{0.026}{(R_1)^{0.18}} \tag{A2}$$

From equations (A1) and (A2)

$$St = \frac{\text{constant}}{(R_1)^{0.18}} = \frac{\text{constant}}{\left(\frac{\rho_1 u_1 x}{\mu_1}\right)^{0.18}} \tag{A3}$$

Therefore, for a given Mach number and wall-temperature ratio a plot of St versus R_1 should have a slope of approximately 0.18. The longer the model or the larger the variation in x the more accurately the slopes can be determined.

APPENDIX B

SIMPLIFIED RELATIONSHIP OF $\frac{St}{St_i}$ TO $\frac{T'}{T_1}$

As has been shown in the discussion of results,

$$St = St' \frac{T_1}{T'} \tag{5}$$

and

$$St' = \frac{0.026}{(R')^{0.18}} \tag{12}$$

These two equations yield

$$St = \frac{0.026}{(R')^{0.18}} \left(\frac{T_1}{T'}\right) = \frac{0.026}{\left(\frac{\rho' u_1 x}{\mu'}\right)^{0.18}} \left(\frac{T_1}{T'}\right) \tag{B1}$$

With the relationships

$$\frac{\rho_1}{\rho'} = \frac{T'}{T_1} \qquad \text{and} \qquad \frac{\mu'}{\mu_1} = \left(\frac{T'}{T_1}\right)^w$$

the equation for St becomes

$$St = \frac{0.026}{\left(\frac{\rho_1 u_1 x}{\mu_1}\right)^{0.18}} \left(\frac{T'}{T_1}\right)^{0.18w-0.82} \tag{B2}$$

or

$$St = \frac{0.026}{\left(\frac{\rho_1 u_1 x}{\mu_1}\right)^{0.18}} \frac{1}{\left(\frac{T'}{T_1}\right)^{0.82-0.18w}} \tag{B3}$$

For the temperature conditions of the tests, w was chosen as 0.8, then

$$St = \frac{0.026}{\left(\frac{\rho_1 u_1 x}{\mu_1}\right)^{0.18}} \frac{1}{\left(\frac{T'}{T_1}\right)^{0.676}} \tag{B4}$$

Since equation (12) applies to incompressible values for St, then

$$St_i = \frac{0.026}{(R_1)^{0.18}}$$

Using this equation for St_i and equation (B4) for St gives

$$\frac{St}{St_i} = \frac{1}{\left(\frac{T'}{T_1}\right)^{0.676}} \tag{B5}$$

REFERENCES

1. Rubesin, Morris W.: A Modified Reynolds Analogy for the Compressible Turbulent Boundary Layer on a Flat Plate. NACA TN 2917, 1953.

2. Sommer, Simon C., and Short, Barbara J.: Free-Flight Measurements of Turbulent-Boundary-Layer Skin Friction in the Presence of Severe Aerodynamic Heating at Mach Numbers From 2.8 to 7.0. NACA TN 3391, 1955.

3. Van Driest, E. R.: Turbulent Boundary Layer Flow in Compressible Fluids. Jour. Aero. Sci., vol. 18, no. 3, March 1951, pp. 145-160, 216.

4. Pappas, C. C.: Measurement of Heat Transfer in the Turbulent Boundary Layer on a Flat Plate in Supersonic Flow and Comparison With Skin-Friction Results. NACA TN 3222, 1954.

5. Brevoort, Maurice J., and Rashis, Bernard: Turbulent-Heat-Transfer Measurements at a Mach Number of 2.06. NACA TN 3374, 1955.

6. Lobb, R. Kenneth, Winkler, Eva M., and Persh, Jerome: Experimental Investigation of Turbulent Boundary Layers in Hypersonic Flow. I.A.S. Preprint No. 452, 1954.

7. Monaghan, R. J., and Cooke, J. R.: The Measurement of Heat Transfer and Skin Friction at Supersonic Speeds. Part III. Measurements of Overall Heat Transfer and of the Associated Boundary Layers on a Flat Plate at $M_1 = 2.43$. R.A.E. TN Aero. 2129, (British), Dec. 1951. (Also available as A.R.C. CP 139, Rep. 15,348, 1953)

8. Fallis, W. B.: Heat Transfer in the Transitional and Turbulent Boundary Layers of a Flat Plate at Supersonic Speeds. UTIA Rep. No. 19, Univ. of Toronto, Inst. of Aerophysics, May 1952.

9. Desmon, Leland G., and Sams, Eldon W.: Correlation of Forced-Convection Heat-Transfer Data for Air Flowing in Smooth Platinum Tube With Long-Approach Entrance at High Surface and Inlet-Air Temperatures. NACA RM E50H23, 1950.

10. Humble, Leroy V., Lowdermilk, Warren H., and Desmon, Leland G.: Measurements of Average Heat-Transfer and Friction Coefficients for Subsonic Flow of Air in Smooth Tubes at High Surface and Fluid Temperatures. NACA Rep. 1020, 1951.

11. DeCoursin, D. G., Bradfield, W. S., and Sheppard, J. J.: Aerodynamic Heating and Heat Transfer Phenomena at Mach Numbers 2.7 Through 5.7. Res. Rep. 101, Univ. of Minnesota, 1954. (Also available as WADC TR 53-379, Feb. 1954)

12. Jack, John R., and Diaconis, N. S.: Heat-Transfer Measurements on Two Bodies of Revolution at a Mach Number of 3.12. NACA TN 3776, 1956.

13. Wilkes, G. B.: Total Normal Emissivities and Solar Absorptivities of Materials. Wright Air Development Center, WADC TR 54-42, March 1954.

14. Douglas, Thomas B., and Dever, James L.: Enthalpy and Specific Heat of Four Corrosion-Resistant Alloys at High Temperatures. Journal of Research of the National Bureau of Standards, vol. 54, no. 1, Jan. 1955, pp. 15-19. (Also NBS Res. Paper 2560)

15. Glasstone, Samuel: Textbook of Physical Chemistry. Second ed., D. Von Nostrand Co., Inc., 1946, p. 415.

16. Chapman, Dean R., and Kester, Robert H.: Turbulent Boundary-Layer and Skin-Friction Measurements in Axial Flow Along Cylinders at Mach Numbers Between 0.5 and 3.6. NACA TN 3097, 1954. (Also available as Jour. Aero. Sci., vol. 20, no. 7, July 1953, pp. 441-448)

17. Clippinger, R. F., Giese, J. H., and Carter, W. C.: Tables of Supersonic Flows About Cone Cylinders, Part 1: Surface Data. BRL Rep. No. 729, Aberdeen Proving Ground, Md., 1950.

18. Sternberg, Joseph: The Transition From a Turbulent to a Laminar Boundary Layer. BRL Rep. No. 906, Aberdeen Proving Ground, Md., May 1954.

19. Rubesin, Morris W.: The Effect of an Arbitrary Surface-Temperature Variation Along a Flat Plate on the Convective Heat Transfer in an Incompressible Turbulent Boundary Layer. NACA TN 2345, 1951.

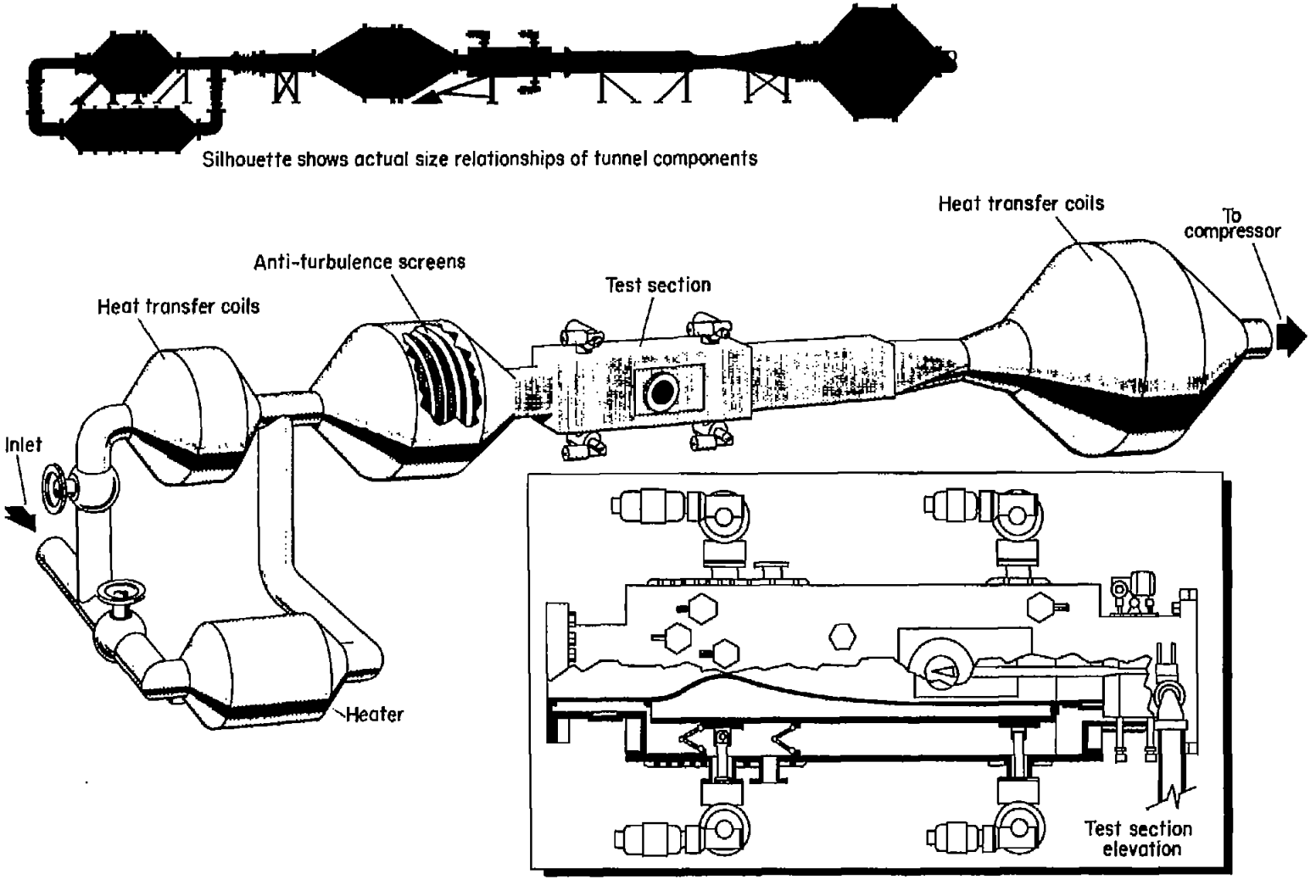

Figure 1.- Schematic drawing of the Ames 10-inch heat transfer wind tunnel.

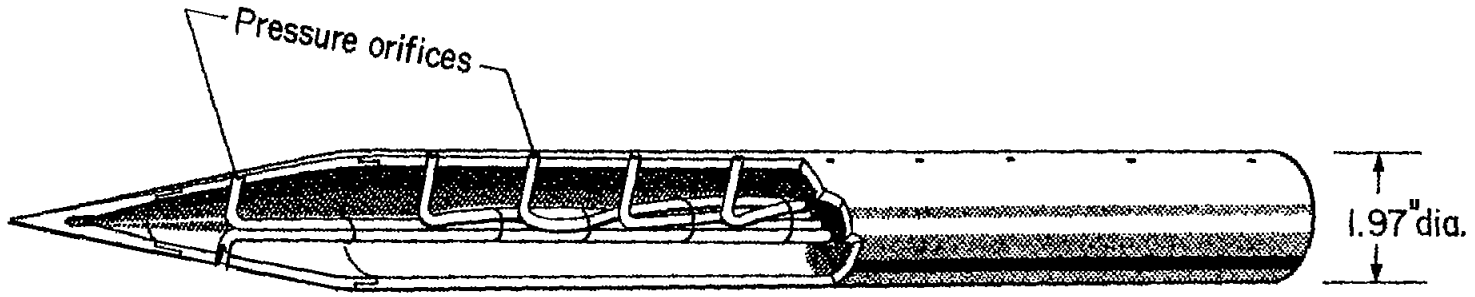

(A) PRESSURE DISTRIBUTION MODEL

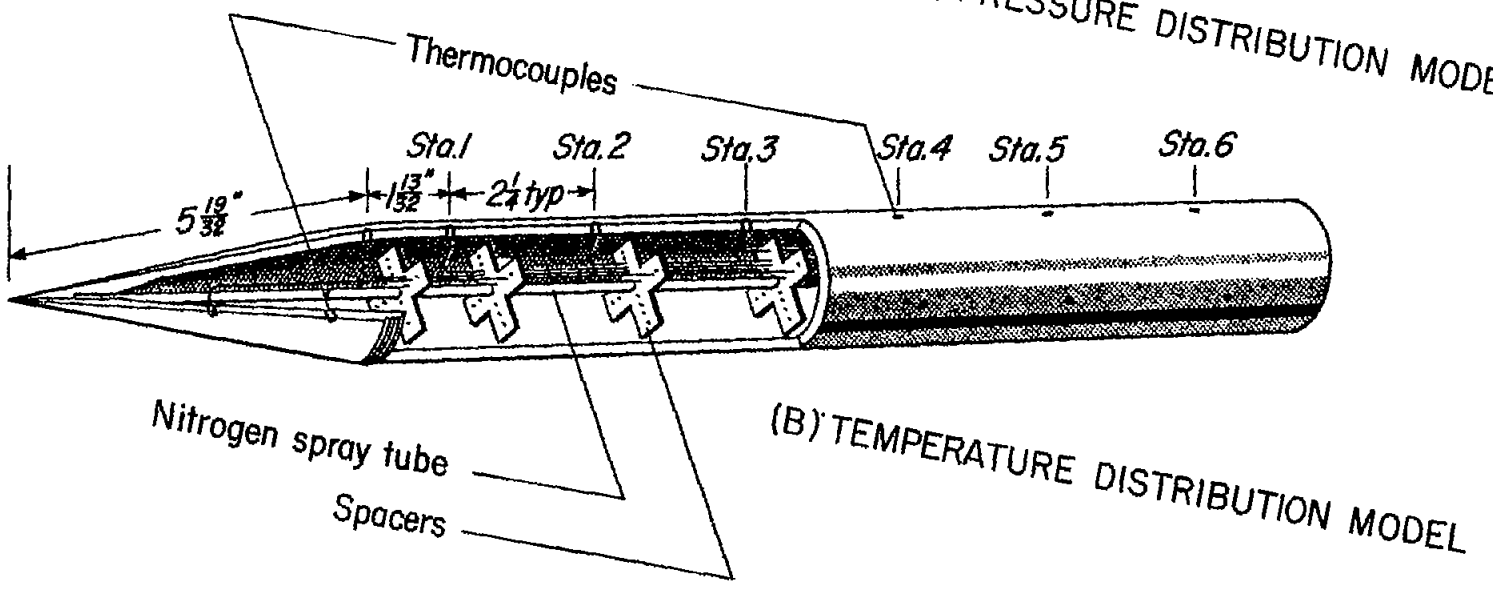

(B) TEMPERATURE DISTRIBUTION MODEL

Figure 2.- Sketch of models.

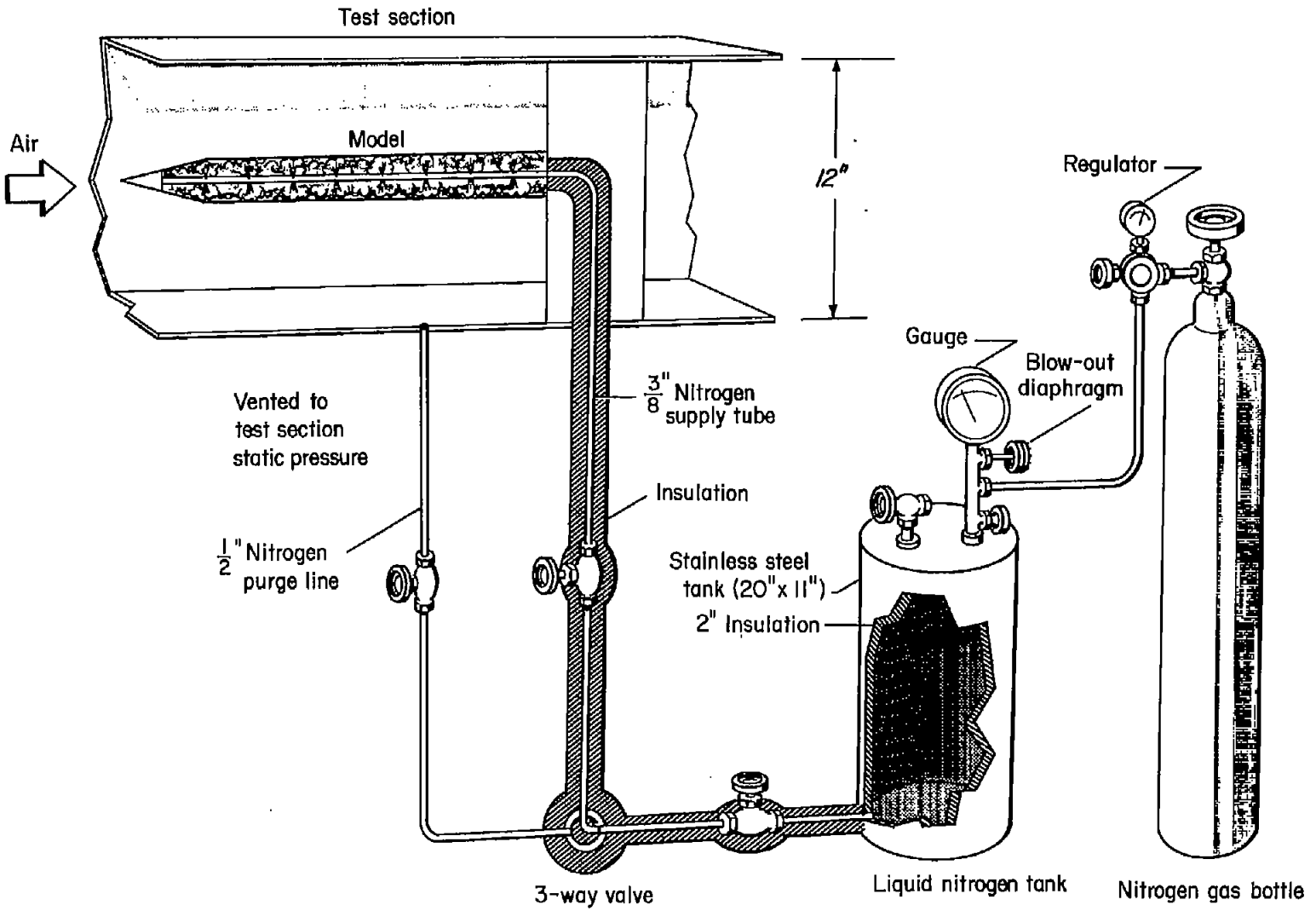

Figure 3.- Equipment used to supply liquid nitrogen to the model.

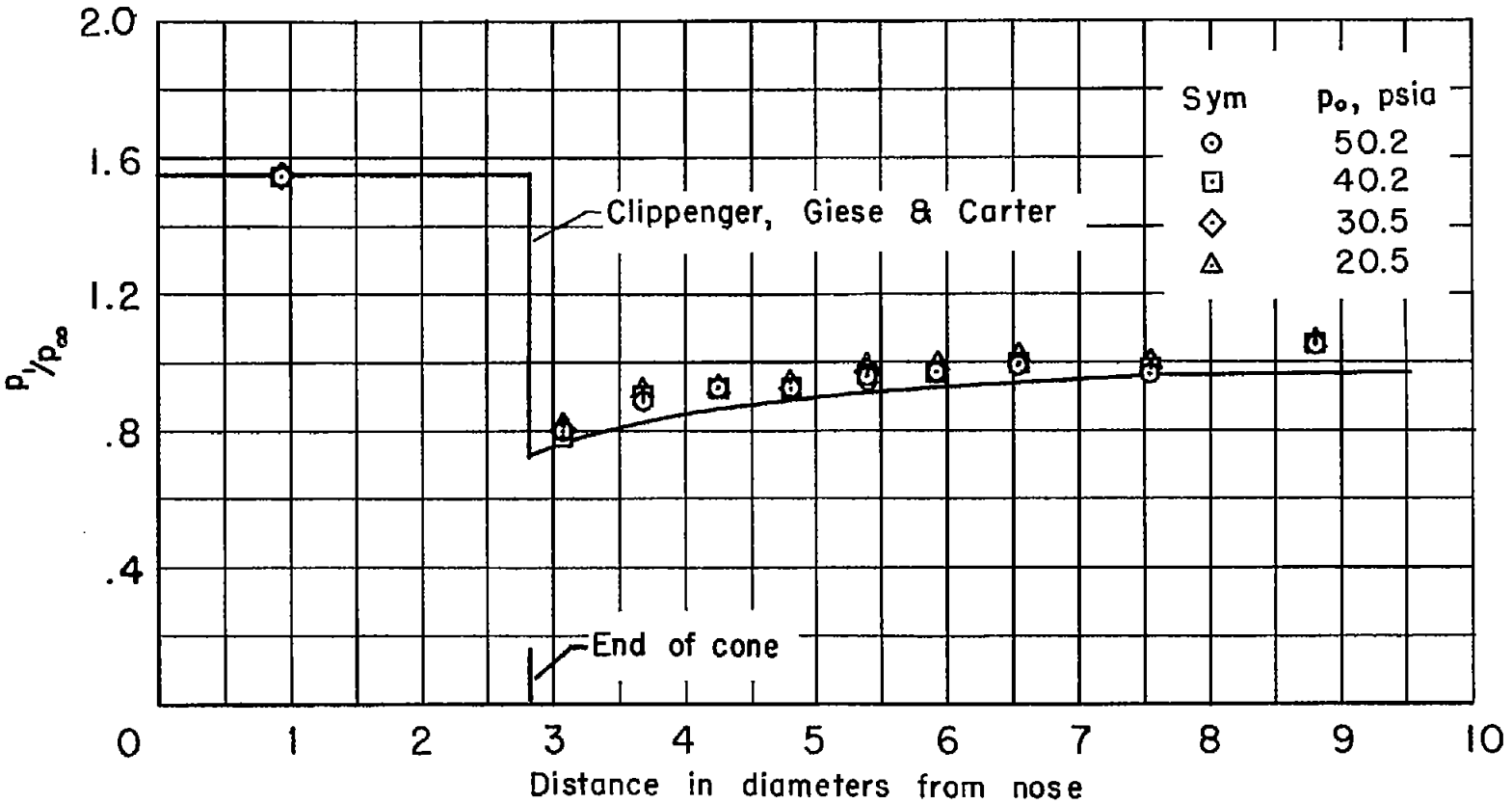

(a) $M_\infty = 3.00$

Figure 4.- Pressure distributions along the model.

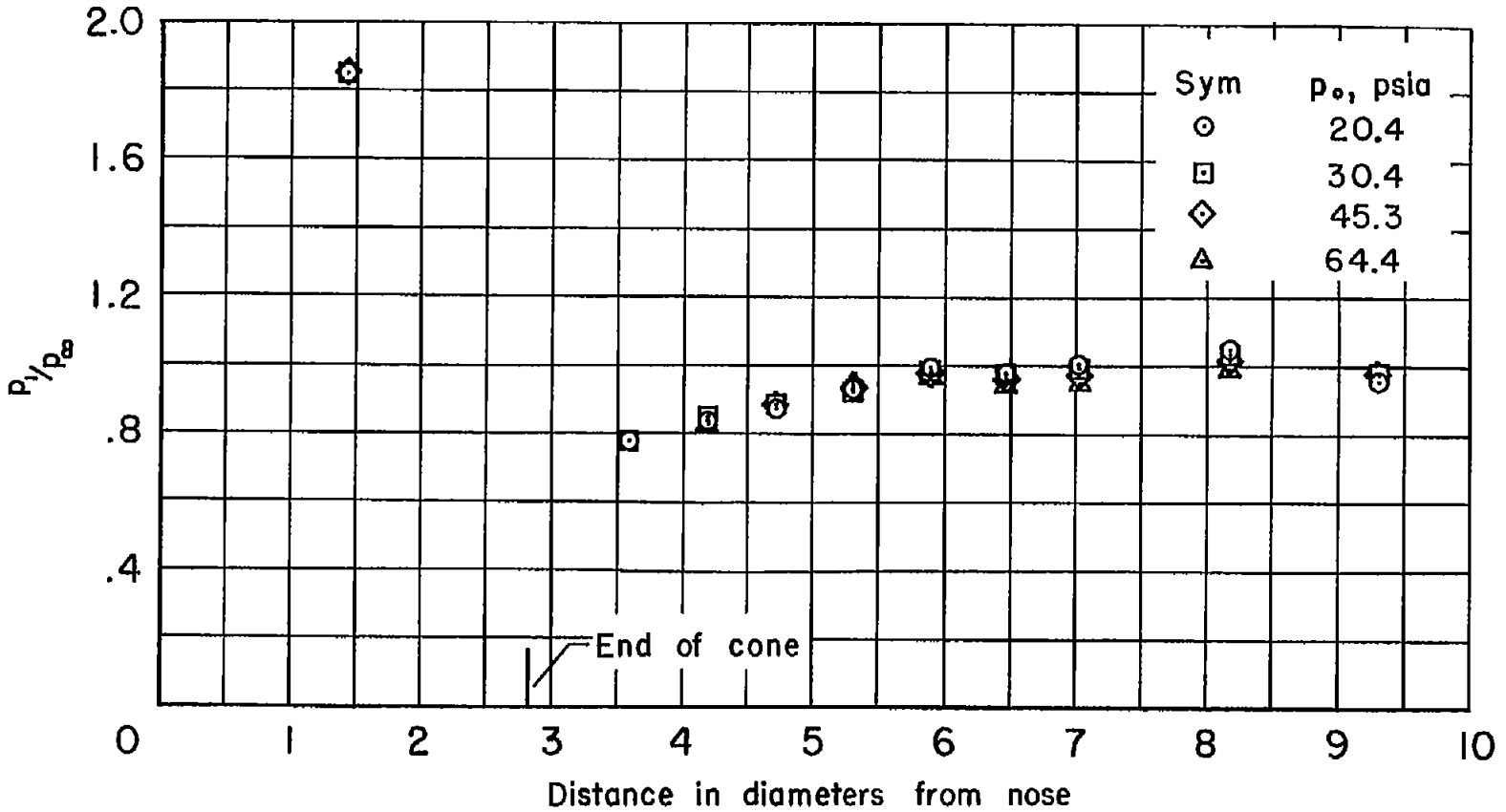

(b) $M_\infty = 3.44$

Figure 4.- Continued.

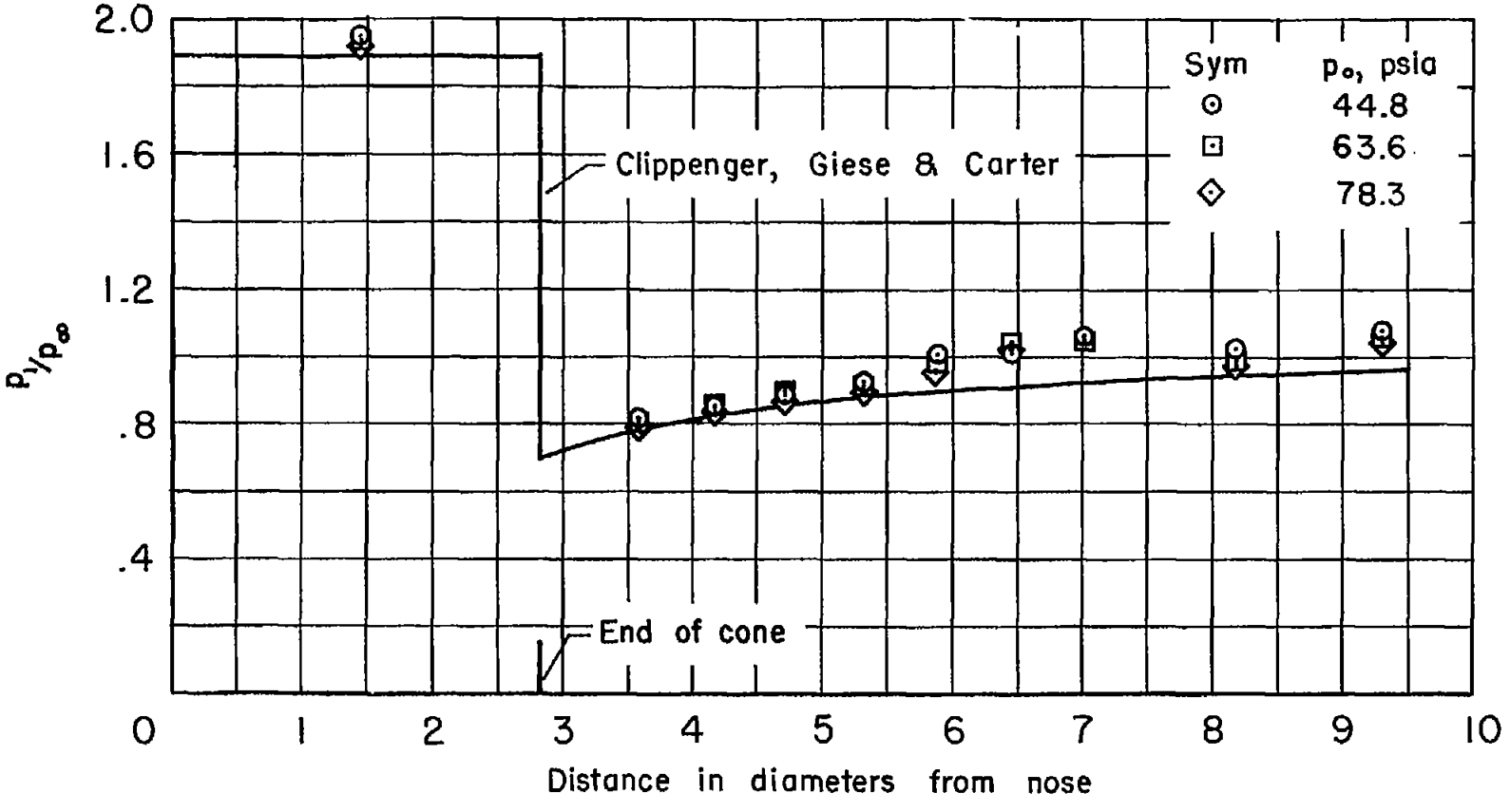

(c) $M_\infty = 4.08$

Figure 4.- Continued.

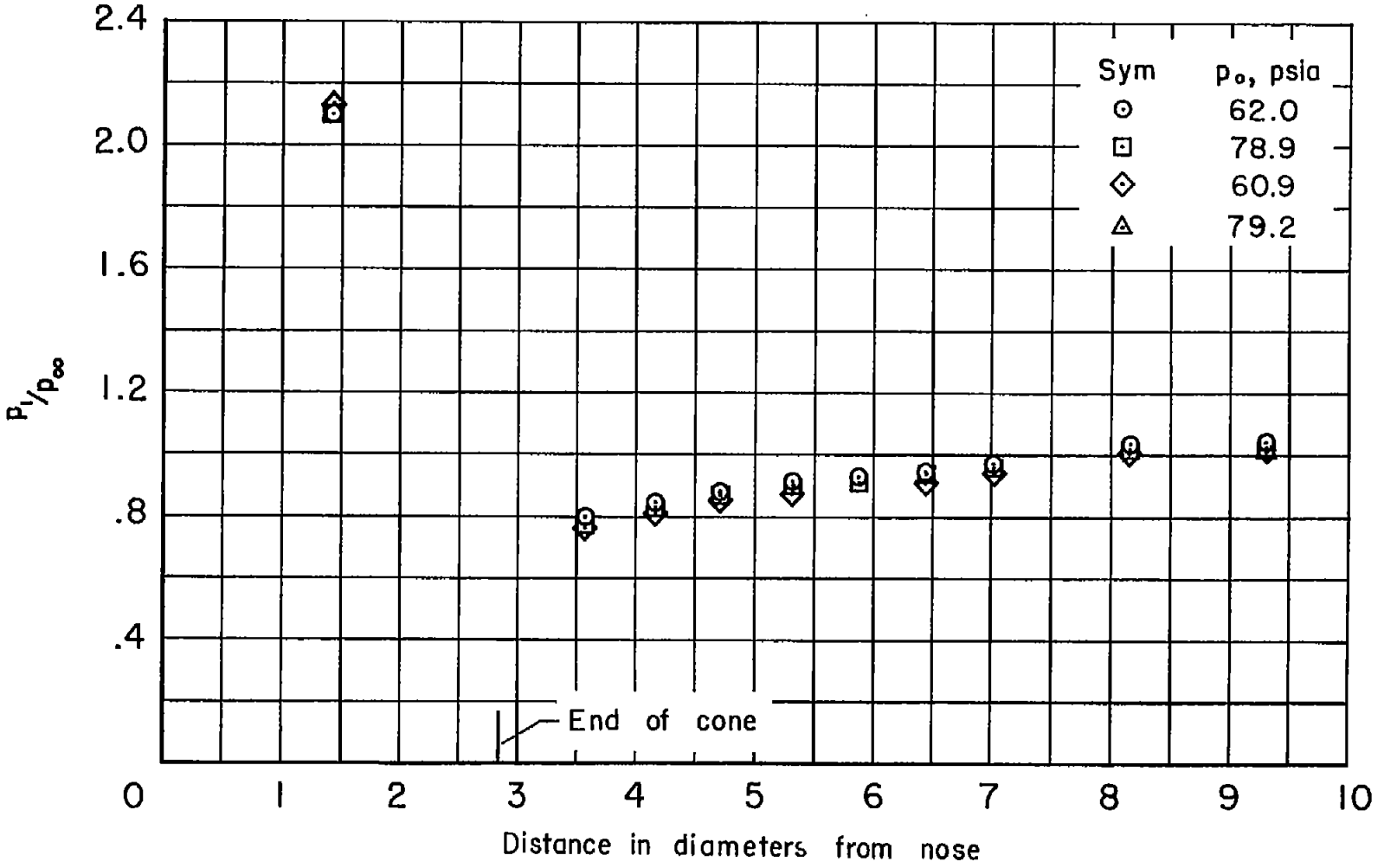

(d) $M_\infty = 4.56$

Figure 4.- Continued.

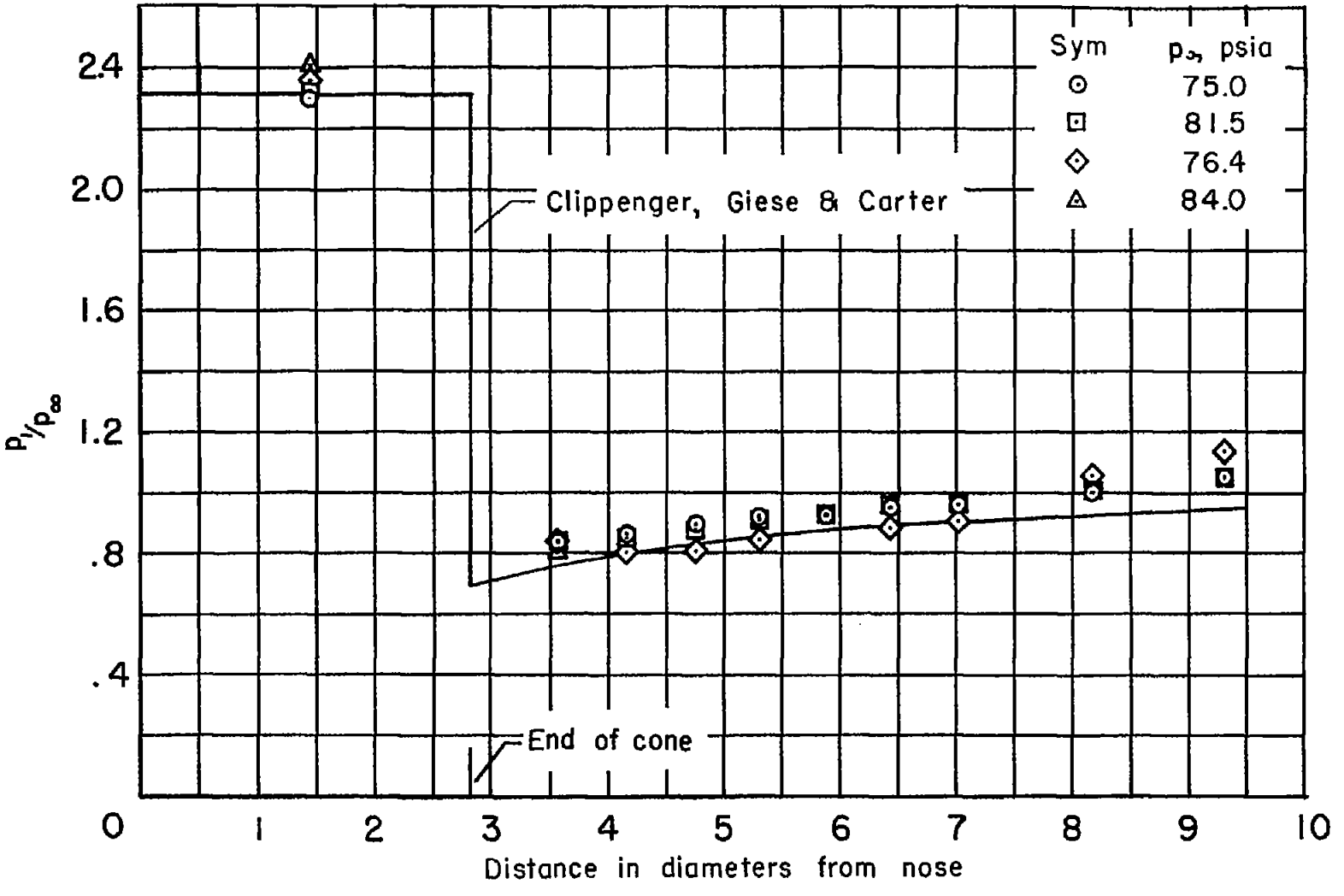

(e) $M_\infty = 5.04$

Figure 4.- Concluded.

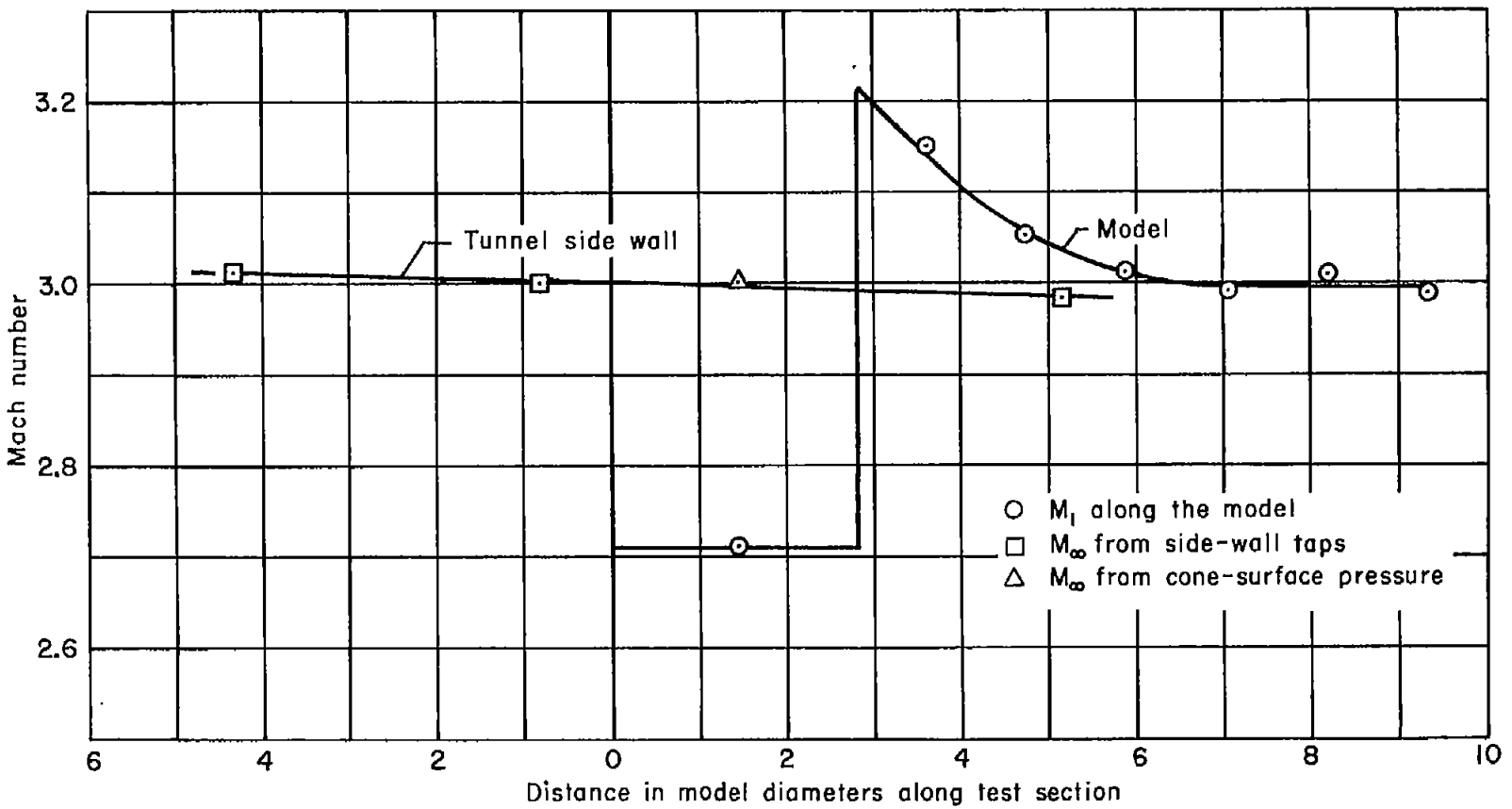

(a) $M_\infty = 3.00$

Figure 5.- Mach number distributions along the model and along the tunnel side wall.

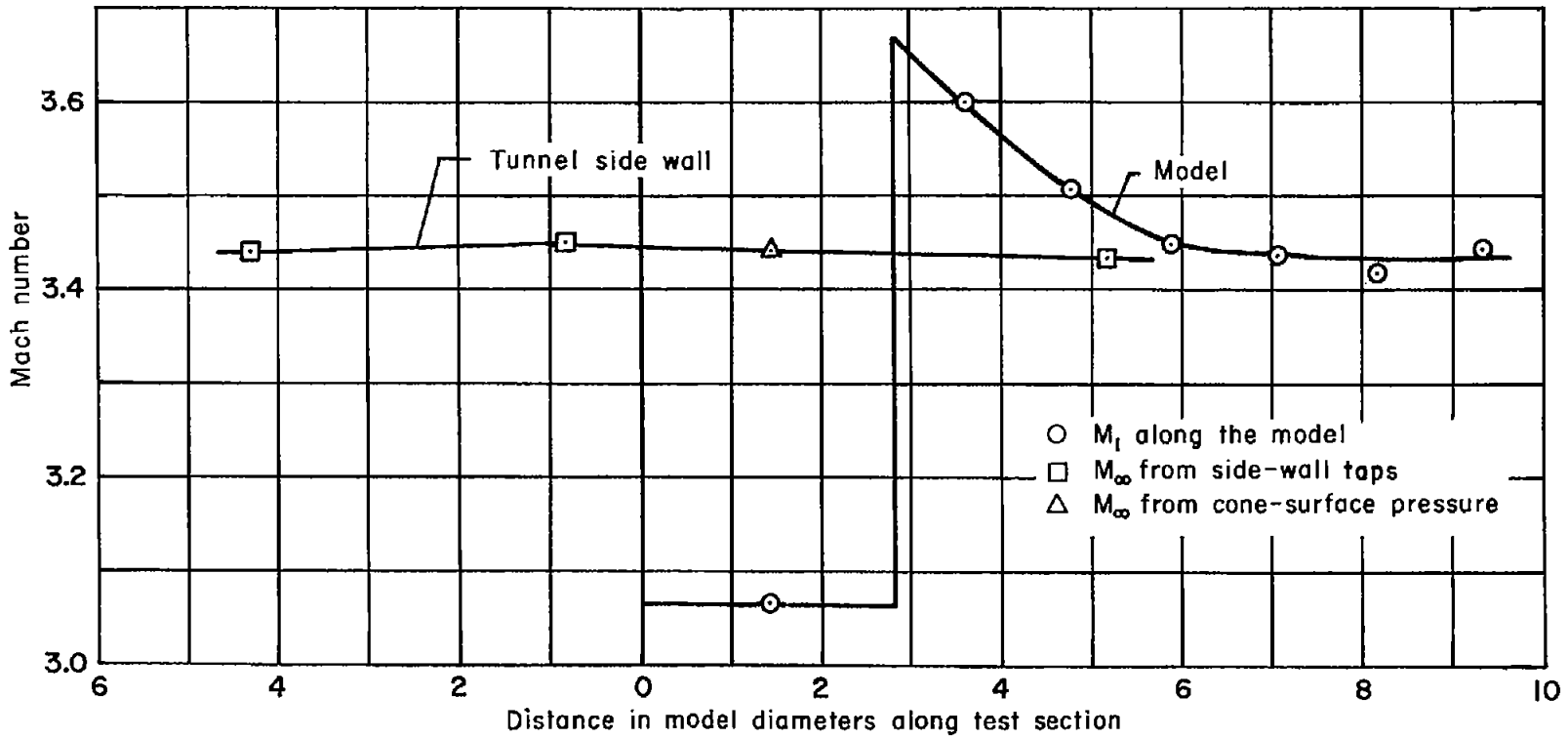

(b) $M_\infty = 3.44$

Figure 5.- Continued.

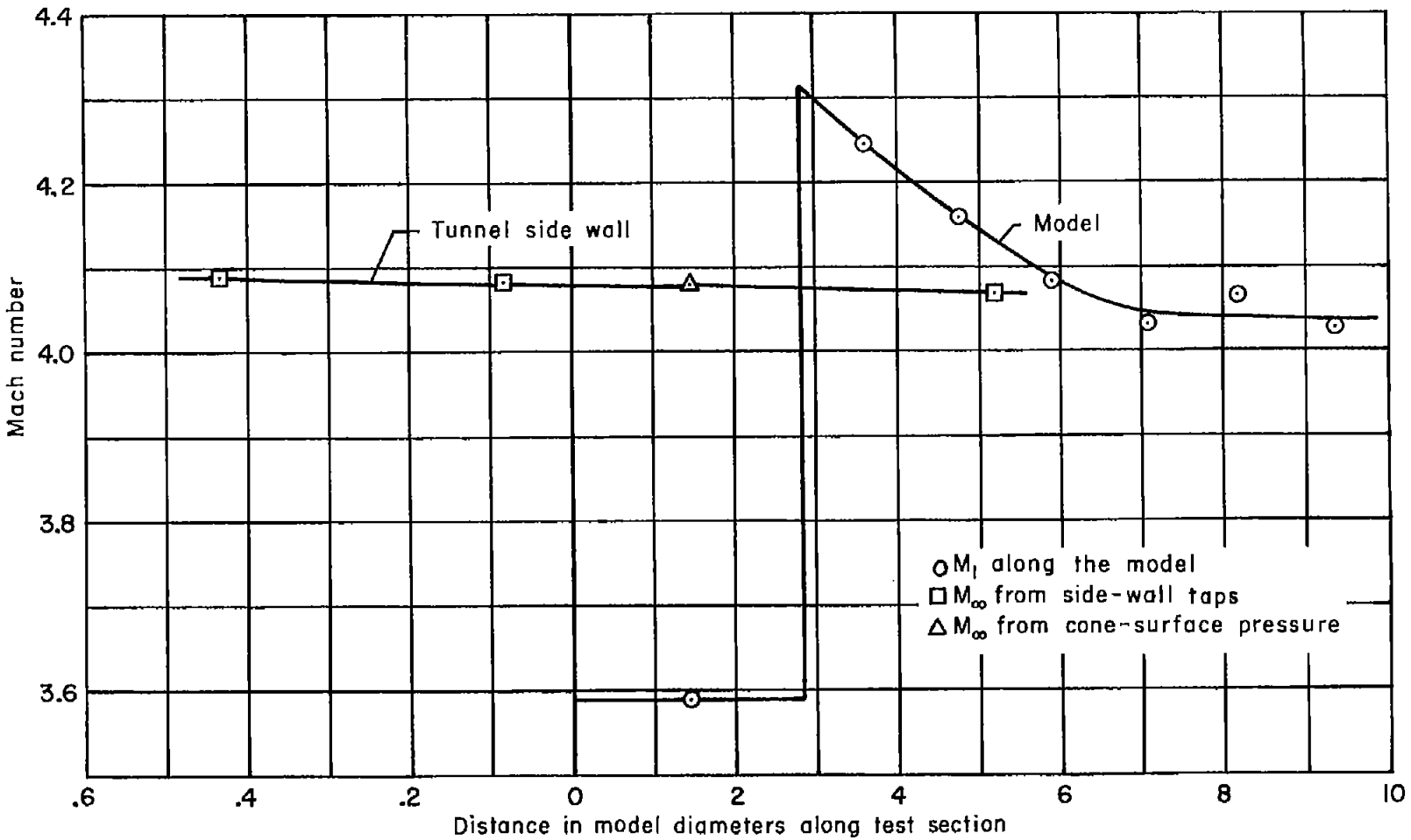

(c) $M_\infty = 4.08$

Figure 5.- Continued.

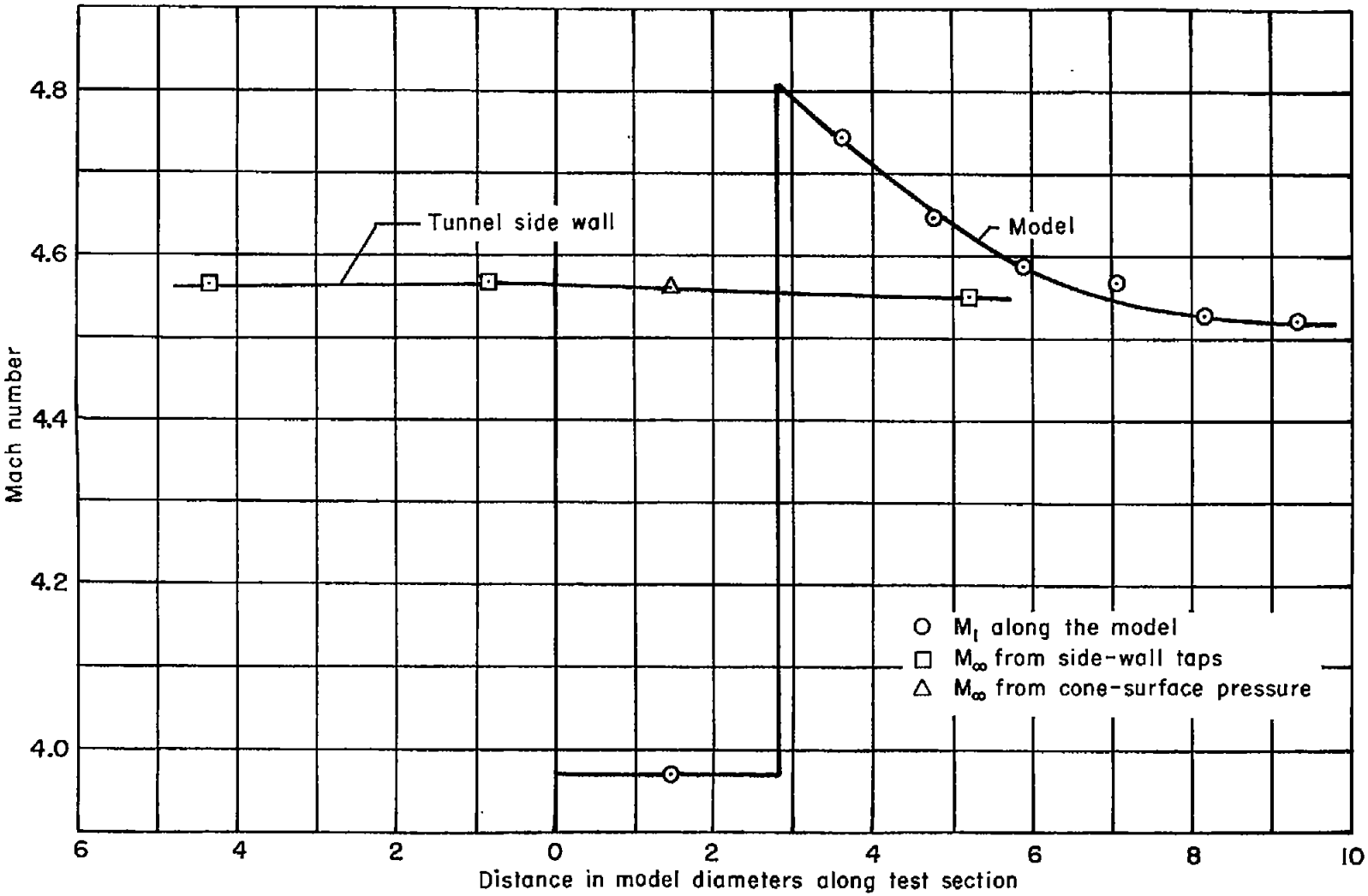

(d) $M_\infty = 4.56$

Figure 5.- Continued.

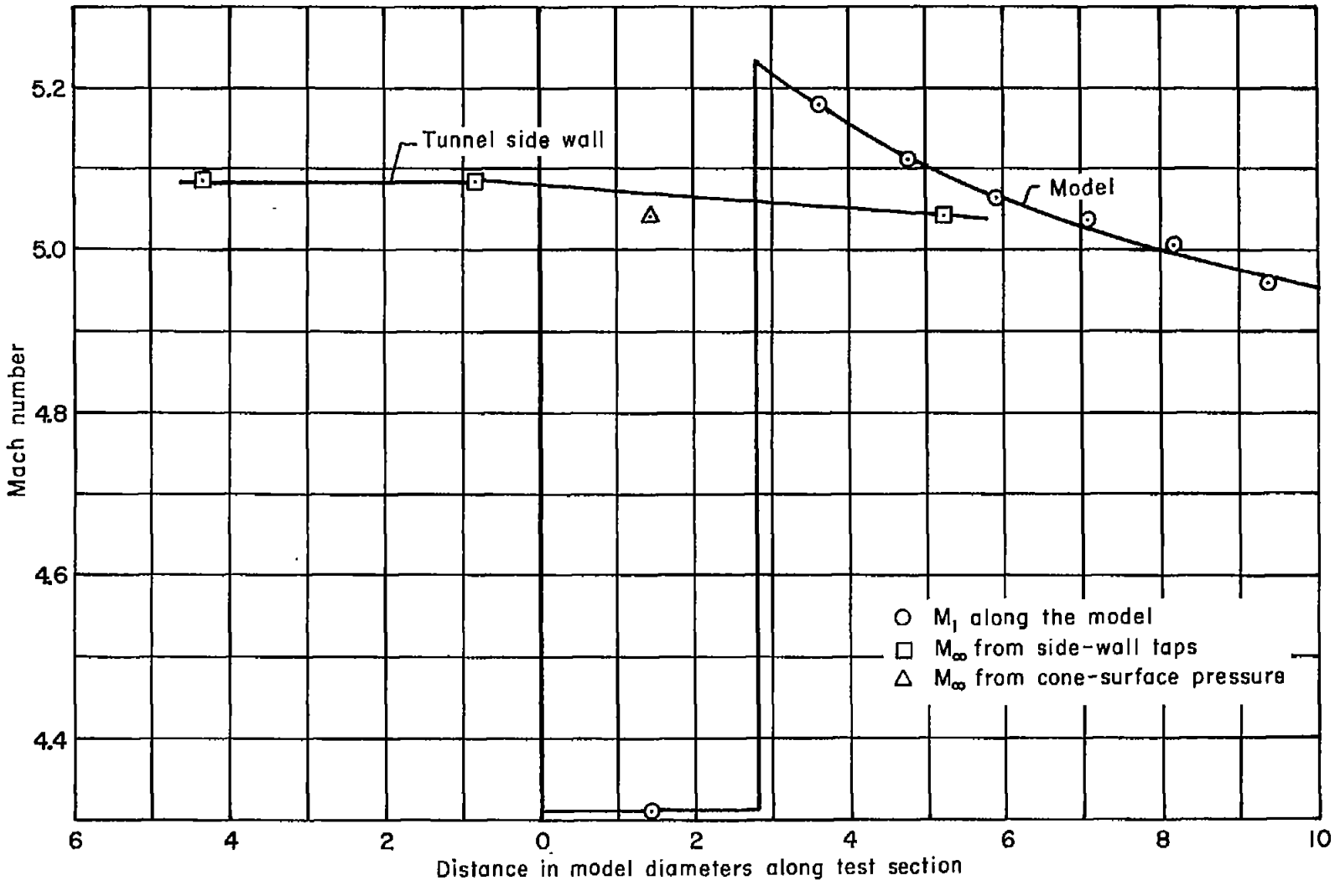

(e) $M_\infty = 5.04$

Figure 5.- Concluded.

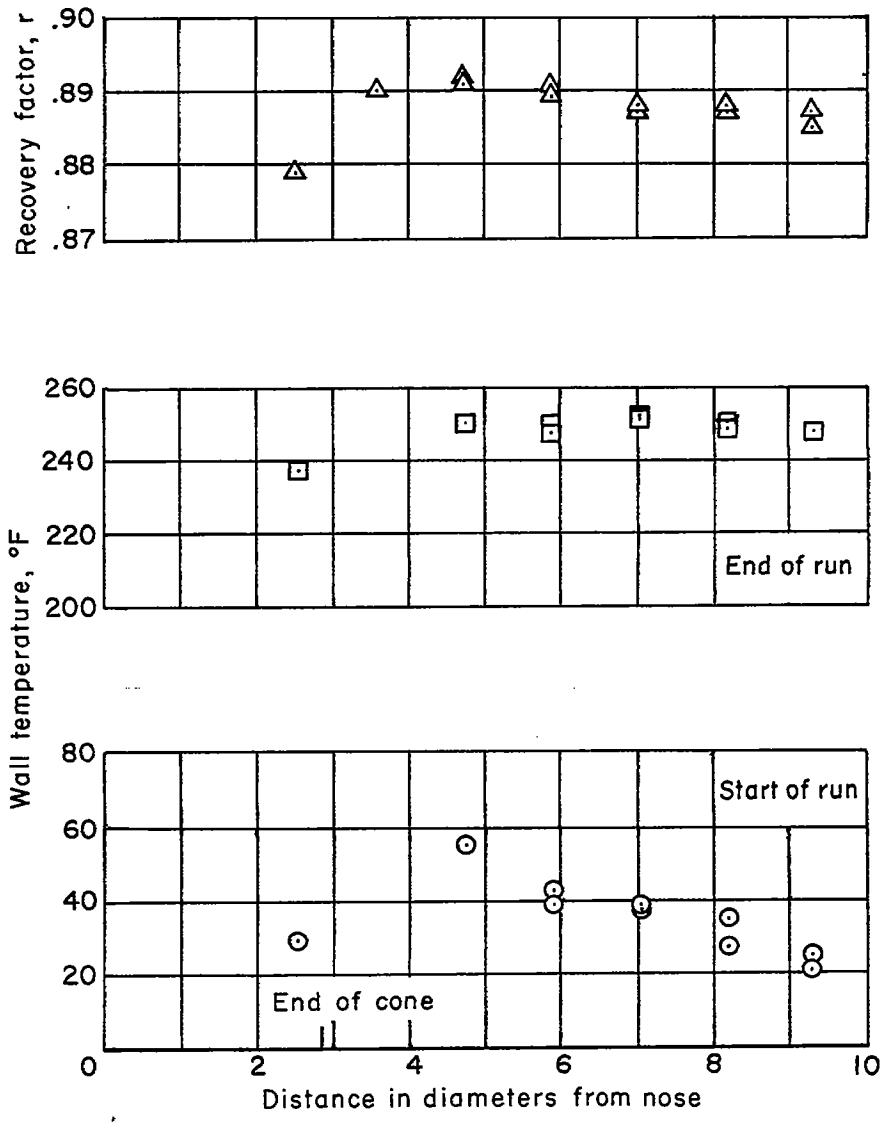

(a) $M_\infty = 3.00$

Figure 6.- Recovery factor and temperature distributions along the model.

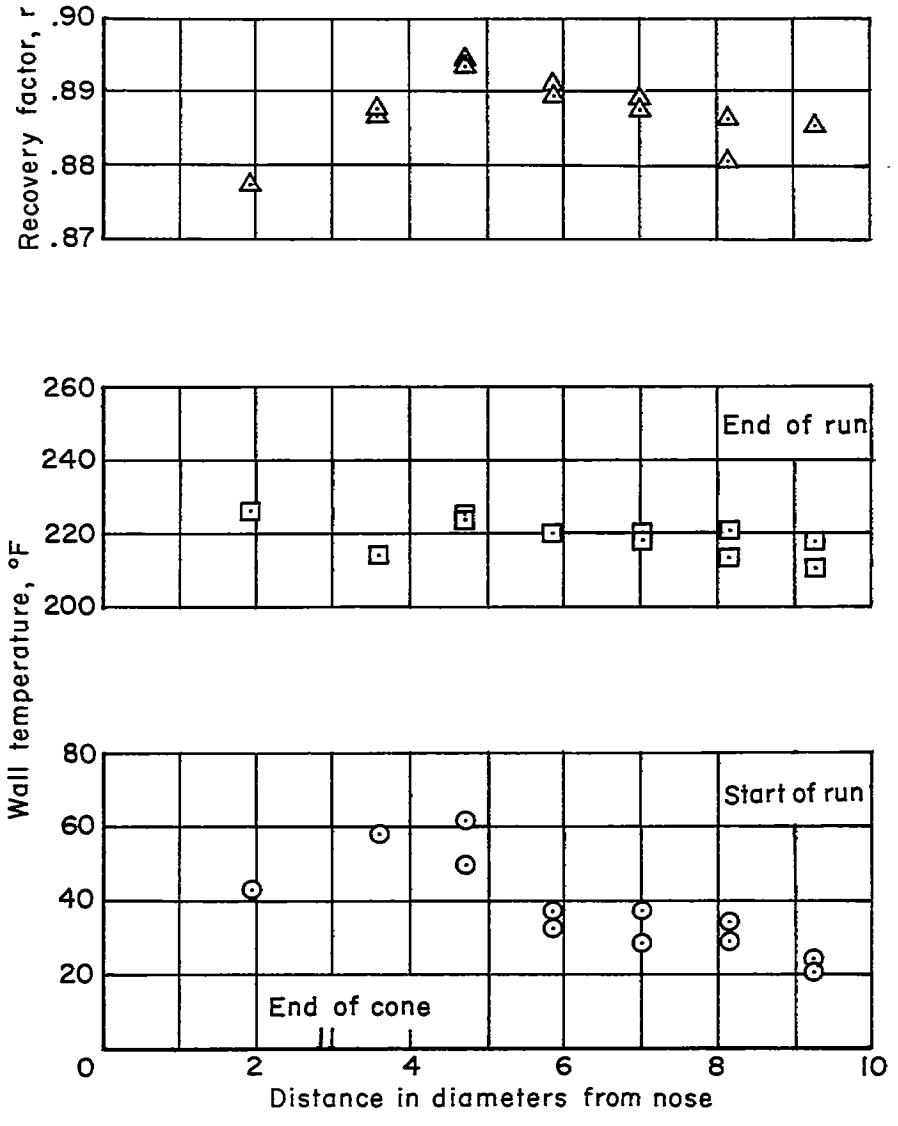

(b) $M_\infty = 3.44$

Figure 6.- Continued.

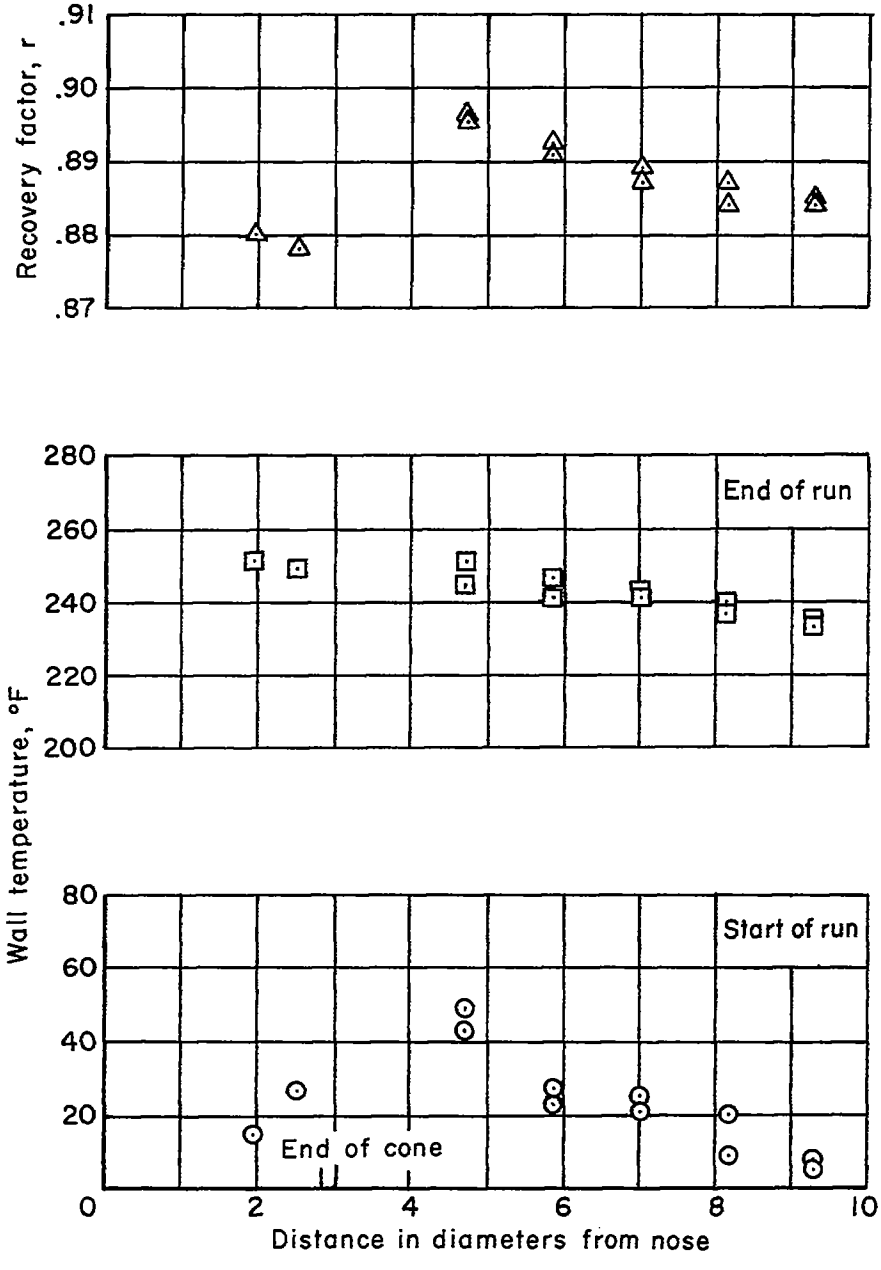

(c) $M_\infty = 4.08$

Figure 6.- Continued.

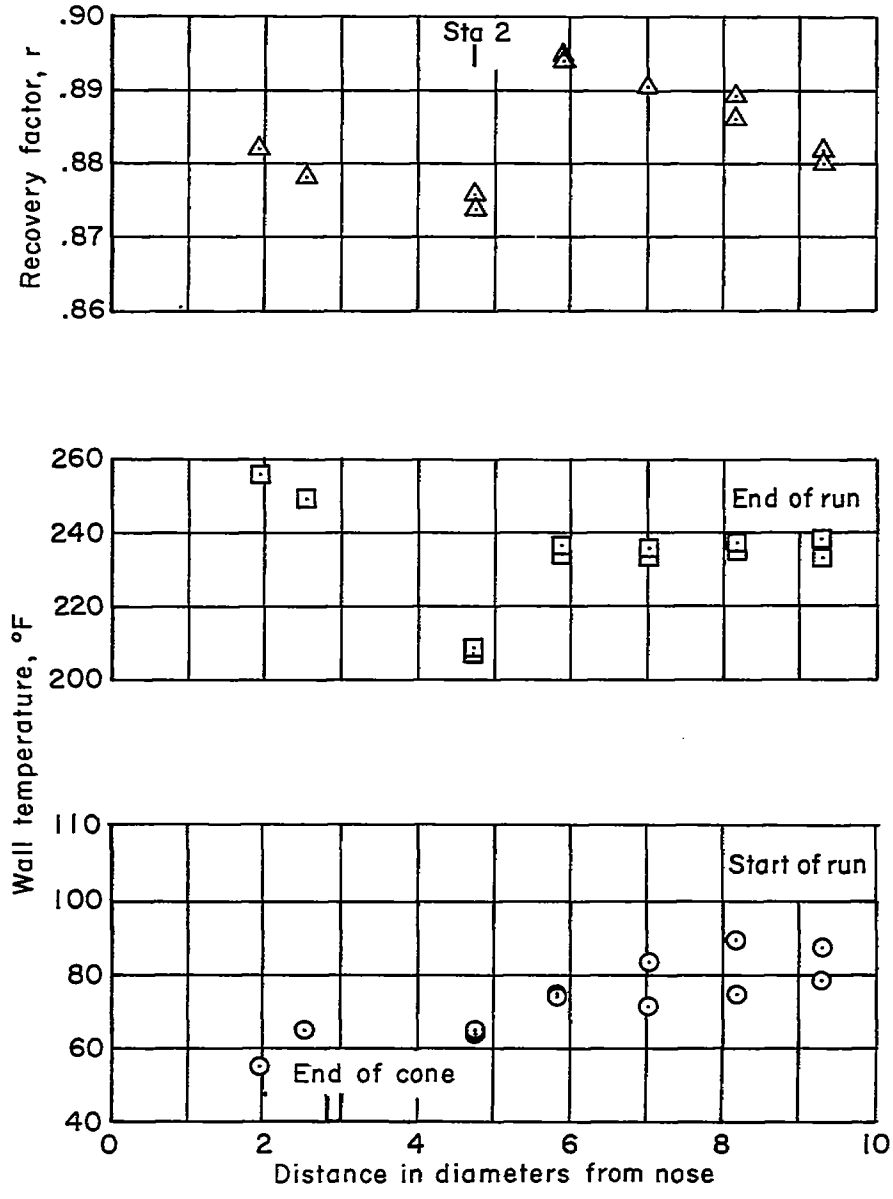

(d) $M_\infty = 4.56$

Figure 6.- Continued.

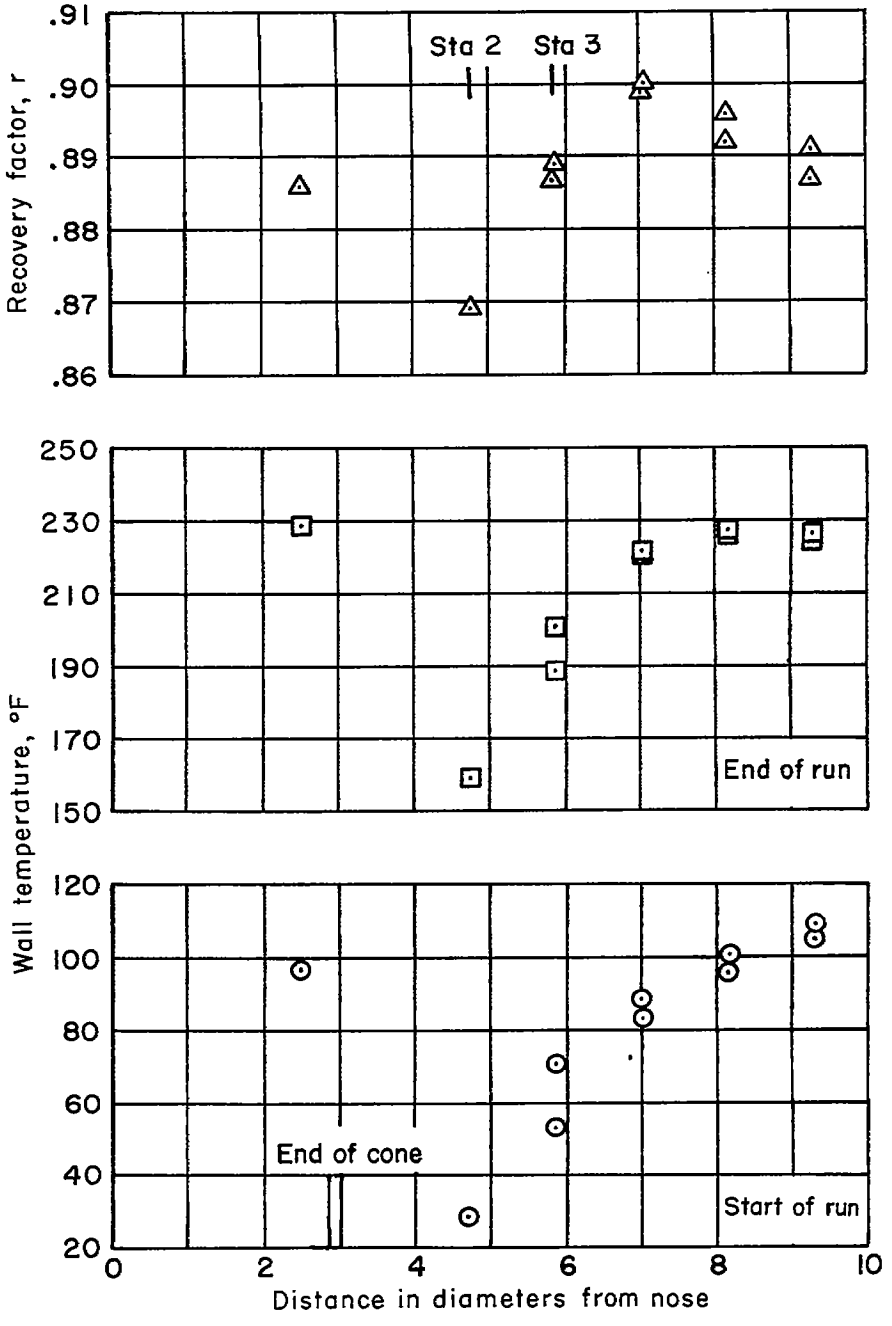

(e) $M_\infty = 5.04$

Figure 6.- Concluded.

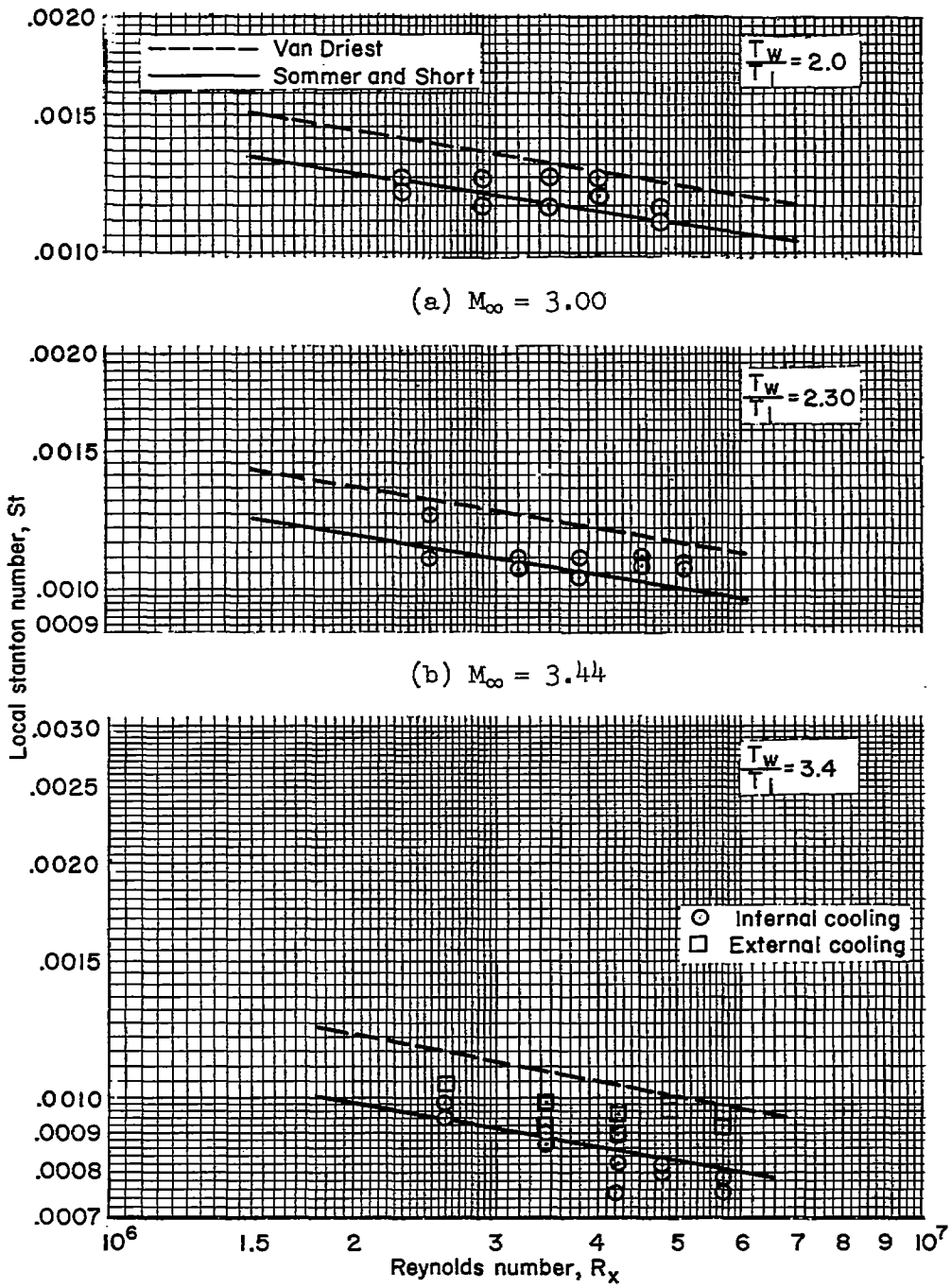

Figure 7.- Typical variation of Stanton number with Reynolds number.

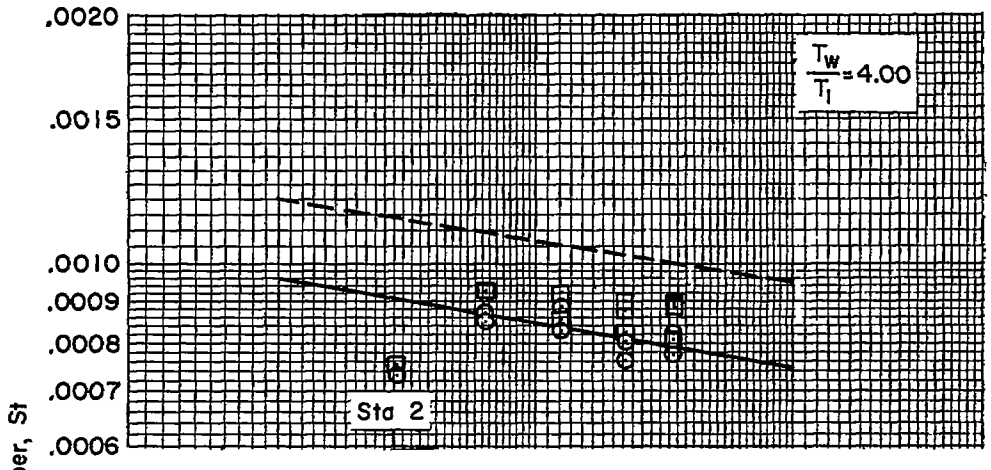

(d) $M_\infty = 4.56$

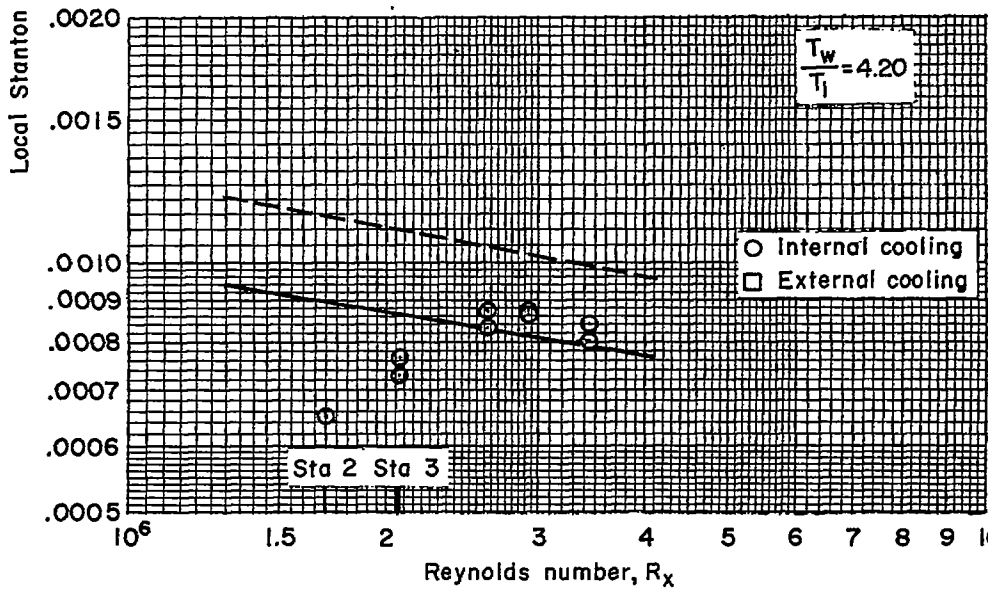

(e) $M_\infty = 5.04$

Figure 7.- Concluded.

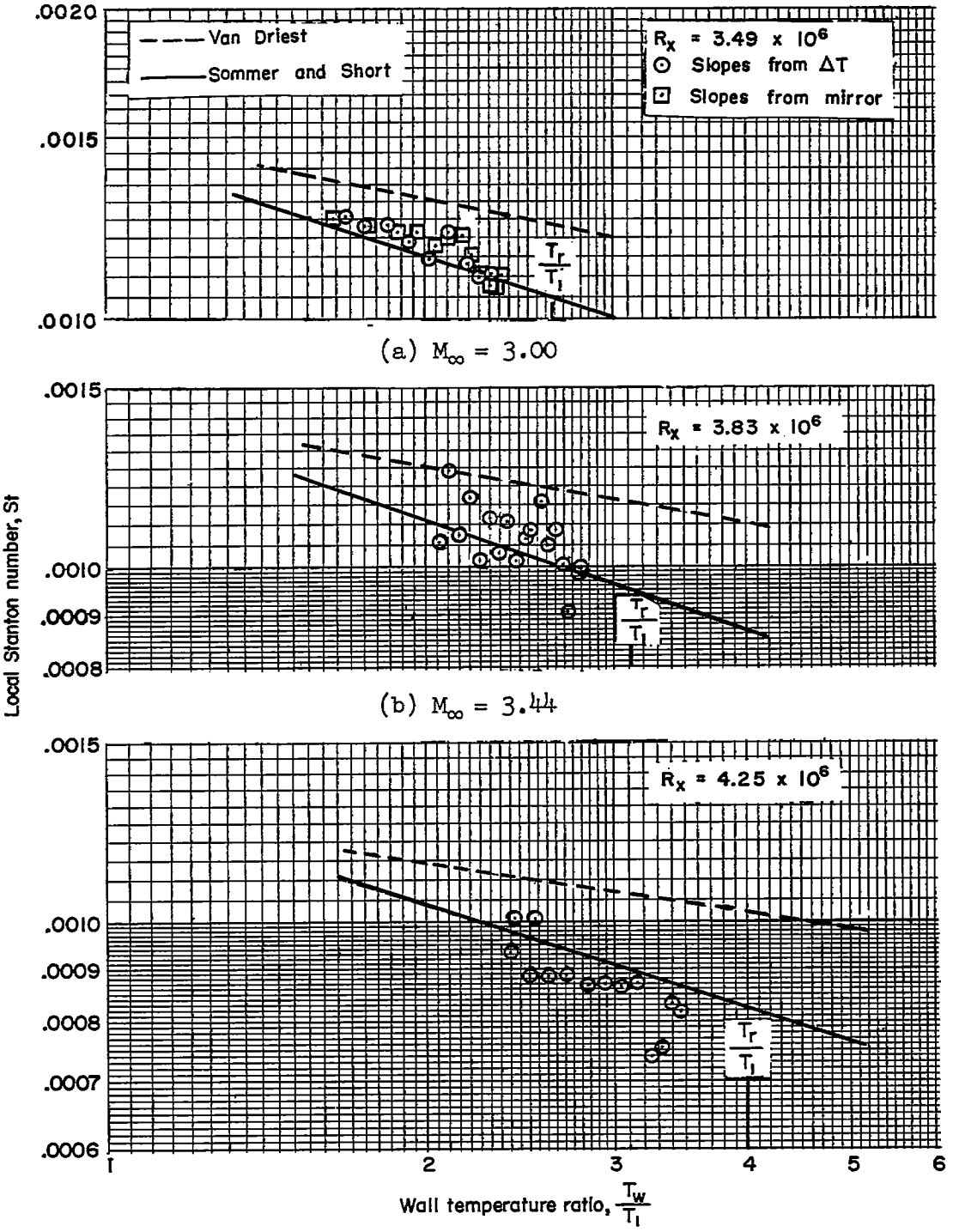

Figure 8.- Typical variation of Stanton number with wall temperature ratio.

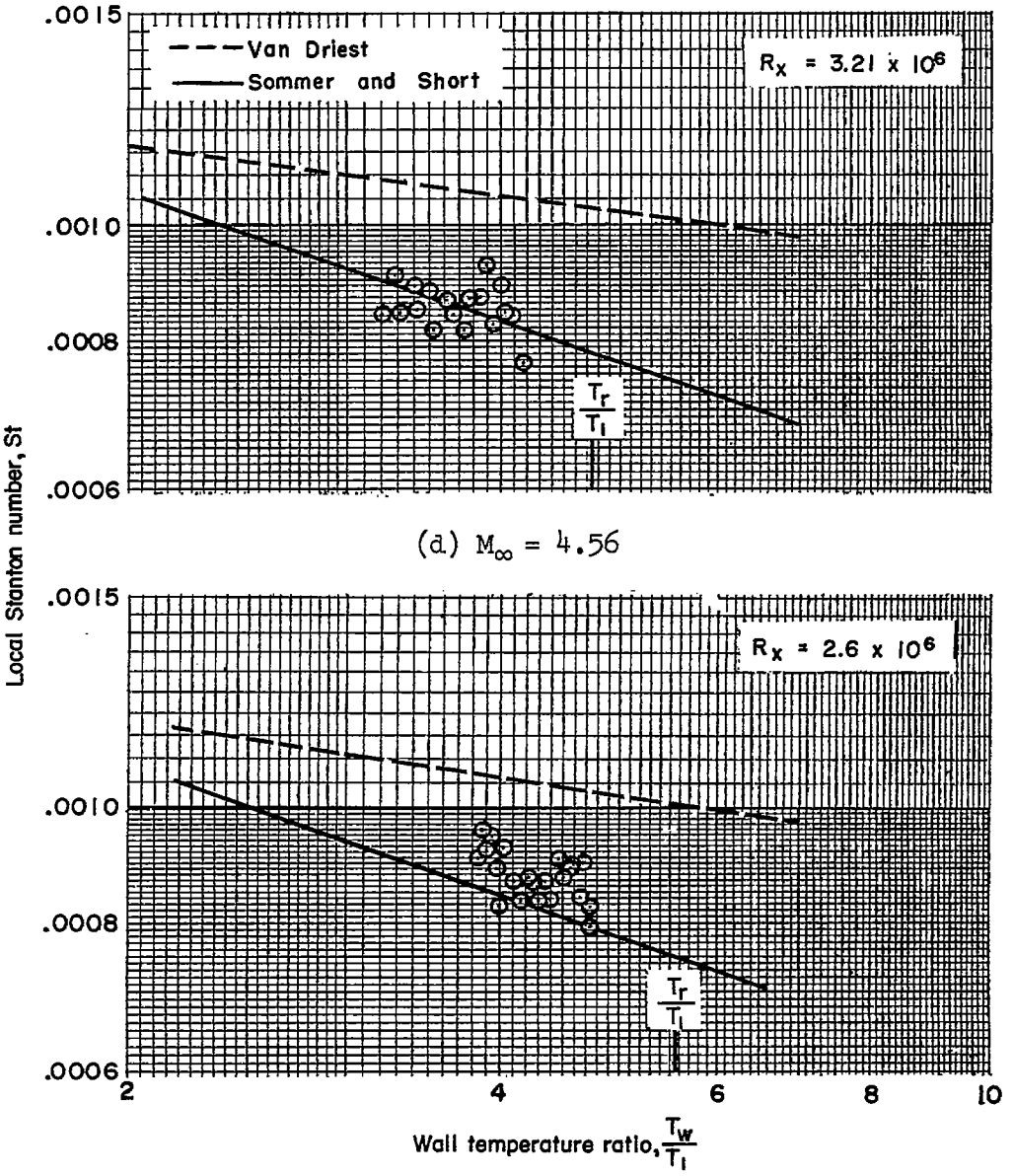

(d) $M_\infty = 4.56$

(e) $M_\infty = 5.04$

Figure 8.- Concluded.

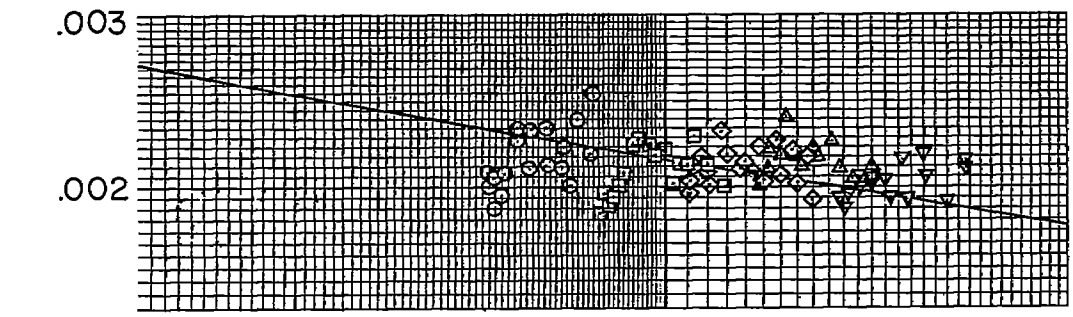

(a) $M_\infty = 3.00$

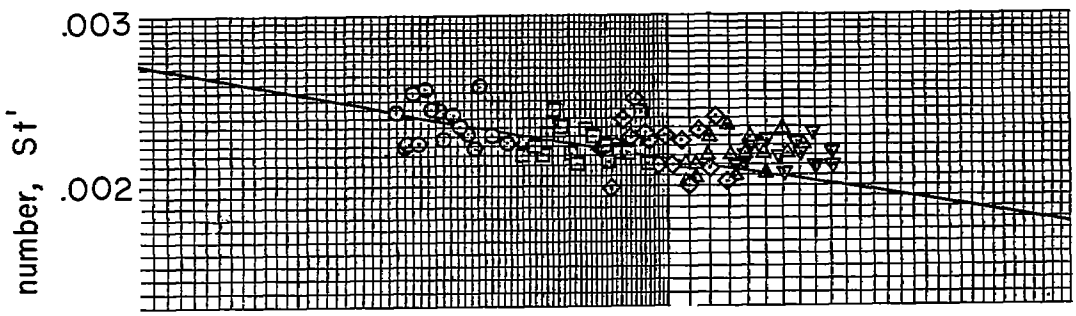

(b) $M_\infty = 3.44$

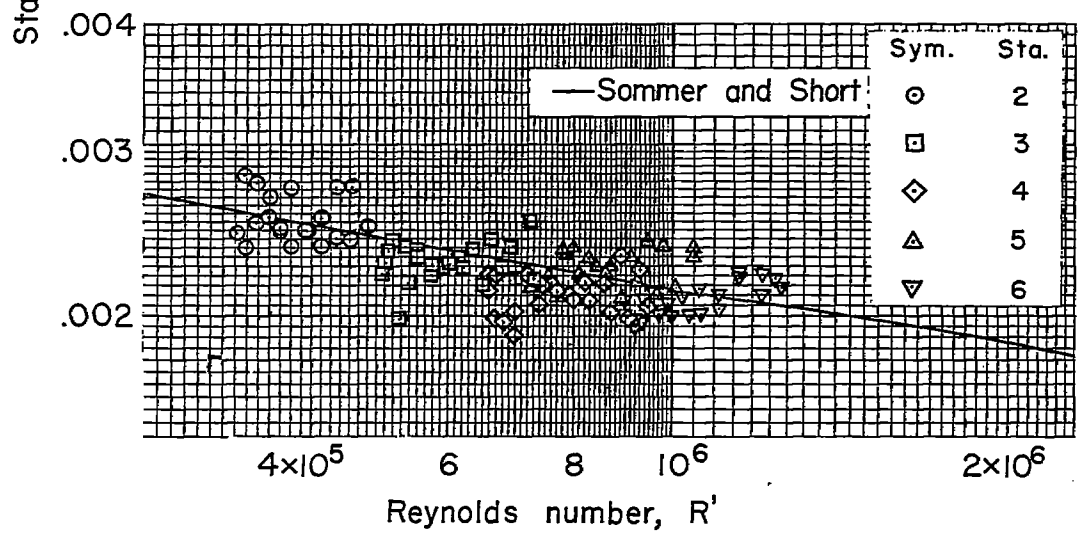

(c) $M_\infty = 4.08$

Figure 9.- Variation of Stanton number with Reynolds number with the properties of air evaluated at a temperature T'.

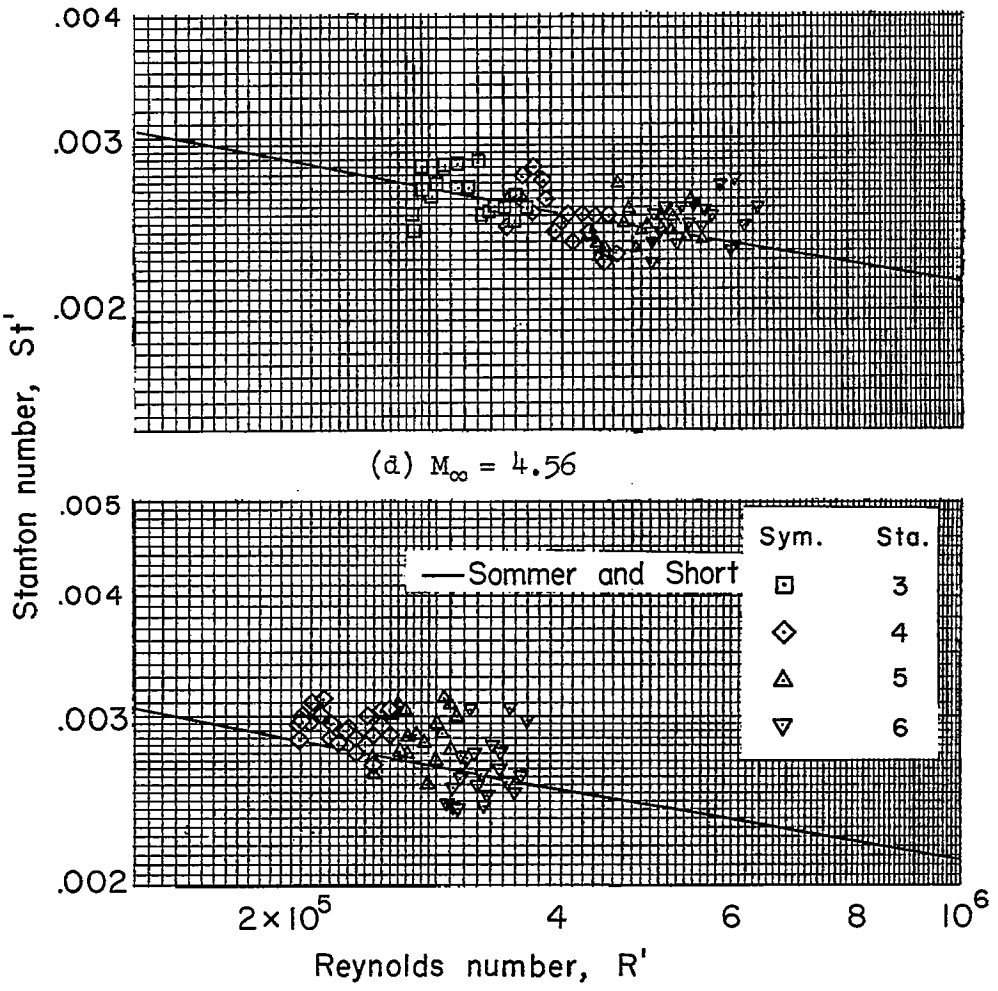

(e) M_∞ = 5.00

Figure 9.- Concluded.

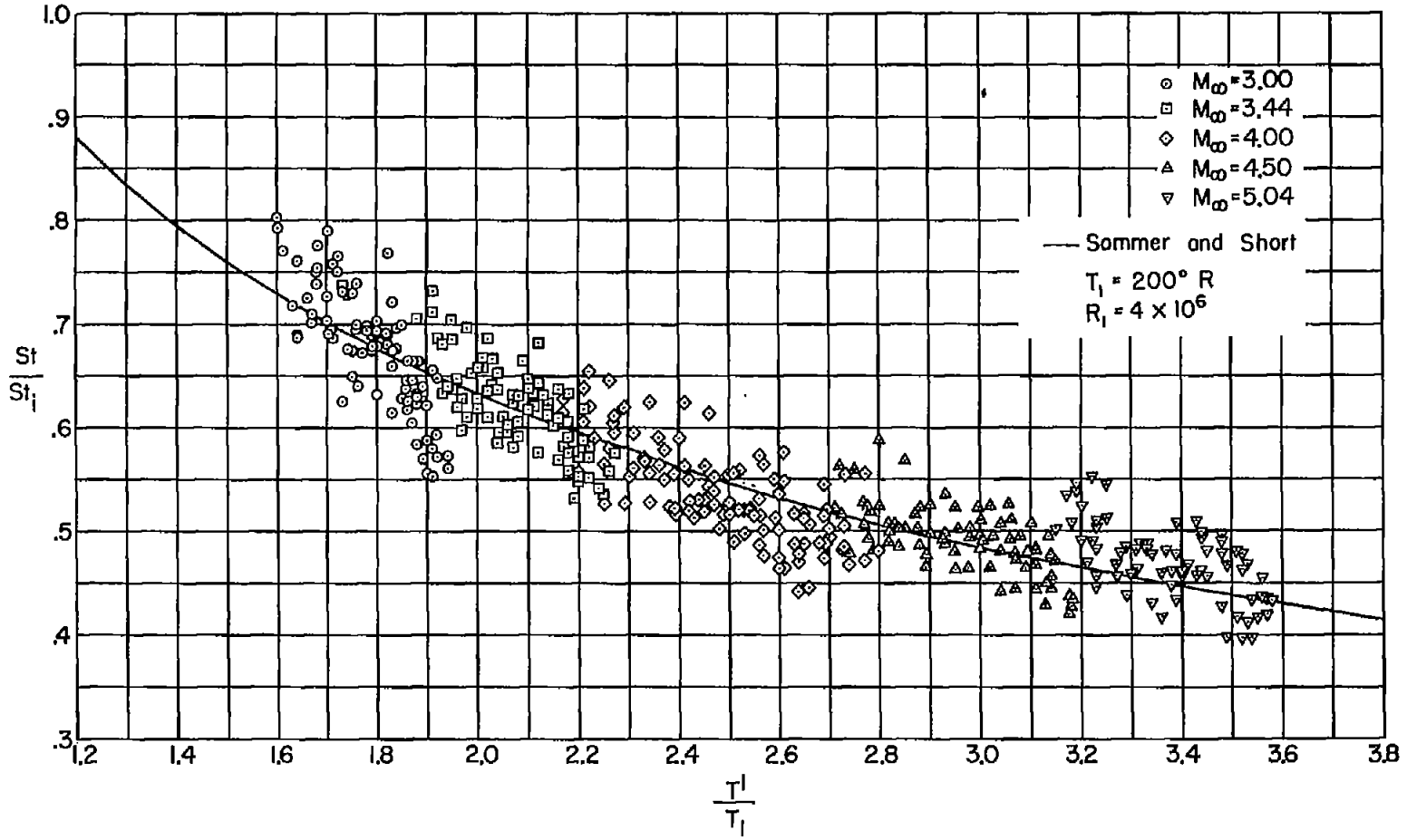

Figure 10.- Comparison of Stanton number ratio with temperature parameter ratio.

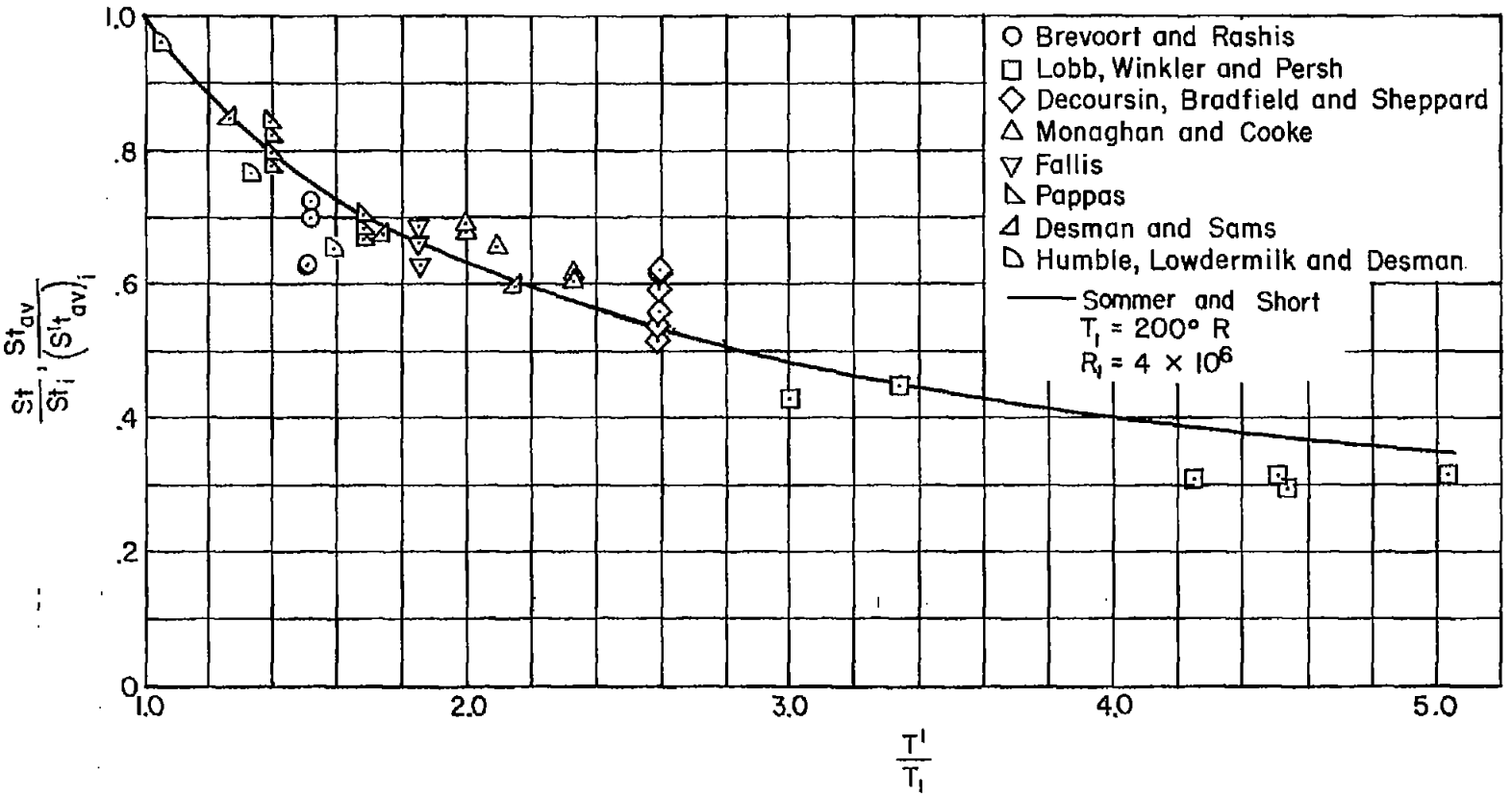

Figure 11.- Comparison of Stanton number ratio with temperature parameter ratio for various investigations.